



# **First-principles Studies of Novel Two-dimensional Materials and Their Physical Properties**



**Yierpan Aierken**

Supervisor: Prof. François M. Peeters

Advisor: Dr. Ortwin Leenaerts

Dr. Deniz Çakır

Department of Physics, University of Antwerp

This dissertation is submitted for the degree of  
*Doctor of Philosophy*

Antwerp, Belgium

June 2017



*I would like to dedicate this thesis  
to my loving parents Arkin and Perwin,  
to my beloved wife Adila Dilshat,  
to my cherished sons Esran and Wildan.*



## **Declaration**

I hereby declare that except where specific reference is made to the work of others, the contents of this dissertation are original and have not been submitted in whole or in part for consideration for any other degree or qualification in this, or any other university. This dissertation is my own work and contains nothing which is the outcome of work done in collaboration with others, except as specified in the text and Acknowledgements. This dissertation contains fewer than 65,000 words including appendices, bibliography, footnotes, tables and equations and has fewer than 150 figures.

Yierpan Aierken  
June 2017



## **Acknowledgements**

And I would like to acknowledge ...



## **Abstract**

This is where you write your abstract ...



# Table of contents

<b>List of figures</b>	xiii
<b>List of tables</b>	xv
<b>1 Introduction</b>	1
1.1 Graphene . . . . .	3
1.1.1 History . . . . .	3
1.1.2 Physical properties . . . . .	6
1.2 Post-graphene materials and their general properties . . . . .	7
1.2.1 Functionalized graphene . . . . .	8
1.2.2 Group IV 2D materials . . . . .	10
1.2.3 2D from layered materials . . . . .	11
1.3 1D from 2D: nanotubes and nanoribbons . . . . .	13
1.4 Synthesis methods . . . . .	16
<b>2 Computational methods</b>	19
2.1 Theory . . . . .	19
2.1.1 Density Functional Theory . . . . .	19
2.1.2 Exchange-correlation functional . . . . .	23
2.2 Implementation . . . . .	28
2.2.1 Software Packages . . . . .	31
<b>3 General physical properties 2D materials</b>	33
3.1 Structural properties . . . . .	33
3.1.1 Layer structure . . . . .	33
3.1.2 sp hybridization . . . . .	37

3.2	Electronic properties . . . . .	39
3.2.1	Graphene . . . . .	40
3.2.2	Dirac cone and symmetry . . . . .	41
3.2.3	Examples: 2D h-BN, 2D MoS <sub>2</sub> and graphene . . . . .	42
3.3	Vibrational properties . . . . .	43
3.3.1	Example: monolayer MoS <sub>2</sub> . . . . .	44
3.3.2	Dynamic stability from phonon dispersion . . . . .	45
3.4	Mechanical properties . . . . .	47
3.4.1	Example: graphene, 2D-BN and 2D-MoS <sub>2</sub> . . . . .	49
3.4.2	Mechanical stability: Born stability criteria . . . . .	49
	<b>References</b>	<b>51</b>

# List of figures

1.1	Graphene publications . . . . .	2
1.2	Relation of graphite, graphene, fullerene and nanotube. Image source: the Nobel prize in physics 2010 [4]. . . . .	4
1.3	Graphene lattice and band structure. . . . .	7
1.4	Atomic and electronic structure of graphane . . . . .	9
1.5	Graphite fluoride to fluorographene. Image source:[46] . . . . .	9
1.6	Buckled hexagonal crystal structures of 2D group IV materials (X = Si, Ge, and Sn). Different colors represent different 2D planes and their distance is the buckling parameter $\delta$ . Image adapted from:[51] . . . . .	10
1.7	Layered hexagonal crystal structures of h-BN. Image adapted from:[65]	12
1.8	Layered structures of TMDs . . . . .	13
1.9	Band structure evolution of MoS <sub>2</sub> from bulk to single layer. Image source: [78] . . . . .	14
1.10	Chiral vector and different type of nanotubes as obtained by rolling them up in different directions. Image adapted from [83] . . . . .	15
1.11	Graphene production setups. Image source [84] . . . . .	16
1.12	Growth of graphene on SiC wafer. Image source [87] . . . . .	17
1.13	A ultra-large-area graphene film. Image source [89] . . . . .	18
2.1	Comparison of the accuracy and the size of electronic structure calculation methods. Image source: [93]. . . . .	20
2.2	Jacob's ladder for DFT approximations. Image source: [99]. . . . .	25
2.3	MAE of the equilibrium lattice constants and band gaps of different functionals on SC40 solid test set <sup>1</sup> . Data source: [102]. . . . .	26

2.4	Schematic illustration of the relation between $E_g$ and $E_g^{KS}$ . Image adapted from: [104]. . . . .	27
3.1	(a) Energy-momentum dispersion relations of single layer and bilayer graphene as approximated by plane intersections of 3D graphite dispersion relation and (b) their 3D dispersion relations around the $K$ k point. (c) Matching of the wavelength in graphite to that in single layer and bilayer graphene. Image adapted from: [115]. . . . .	35
3.2	Energy-momentum dispersion relations of MoS <sub>2</sub> as plane intersections of 3D dispersion relations. Image adapted from: [117]. . .	36
3.3	Three types of sp hybridized orbitals. Image adapted from: [119]. . . . .	38
3.4	The formation of $sp^2 \sigma$ and $p_z \pi$ double bond. Image source: [122]. . . . .	40
3.5	Graphene lattice and its Brillouin zone. Image source: [14]. . . . .	41
3.6	Possible positions for the second atom (blue area) in order to guarantee the existence of Dirac cones as going from (a) square lattice to (f) hexagonal lattice. The first atom is located at the corners of the unit cell. Image source: [123]. . . . .	42
3.7	Electronic band structures of 2D-hBN, 2D-MoS <sub>2</sub> and graphene calculated with PBE-GGA functional. . . . .	42
3.8	(a) phonon modes of layered bulk (first row) and monolayer (second row) MoS <sub>2</sub> at $\Gamma$ q point. (b) phonon dispersion and projected DOS of monolayer MoS <sub>2</sub> . . . . .	46
3.9	Imaginary frequencies are shown as negative frequencies in a phonon dispersion plot. . . . .	46
3.10	(a) A structure at the convex (left) and the concave (right) of the PES. (b) Searching for a stable structure (phase transition). . . . .	47

# **List of tables**

3.1	Mechanical properties of graphene, BN and MoS <sub>2</sub> . . . . .	49
-----	----------------------------------------------------------------------	----



# **Chapter 1**

## **Introduction**

A new field of research related to both material science and condensed matter physics has been formed since the synthesis of graphene in 2004 [1, 2]. Graphene is a sheet of carbon atoms in a crystal form having a single atom thickness. Given the thin plane-like structural nature of this type of material the field is named two-dimensional (2D) material. The synthesis itself together with the phenomenal properties of graphene has led to a Nobel Prize in physics awarded to Andre Geim and Konstantin Novoselov in 2010 [3]. Since then, the field is expanding with the involvement of researchers not only from young community, but also from experts who have been working on graphene-related materials like graphite, fullerenes and carbon nanotubes. As a result, researches focused on graphene and related topics increasing with unprecedented speed, see Fig. 1.1. While part of the research has been to explore more the properties of graphene itself and its applications, the other related research has been conducted on discovering new 2D materials. It has been evidenced from graphene, same material having different dimensionality can have different properties. For example, as compared to graphite, its monolayer graphene has a superior mechanical properties and massless carriers, to name a few. Therefore, many materials with hidden properties which will only manifest themselves at other dimensions are yet to be discovered.

On the other hand, with the advent of powerful supercomputer facilities, calculations that seems impossible to finish in a reasonable time now has been made possible. The accuracy of such calculations is the most crucial aspect of computational physics, especially when the results are utilized to predict real

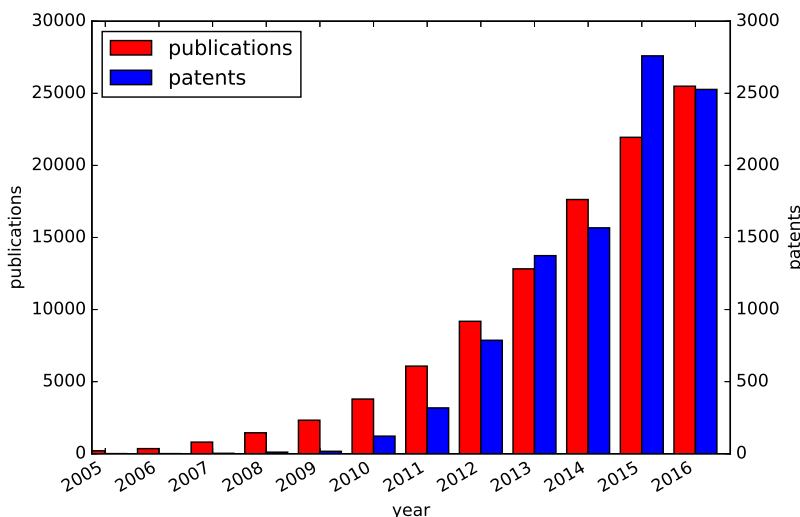


Fig. 1.1 Graphene related publications and patents during the last decade. Data source: ISI Web of Science and PATENTSCOPE.<sup>1</sup>

materials properties. To make the time spent on costly supercomputer valuable, researchers and programmers have been making important progress in order to make sure theories and its implementation are correct and the results they yield are within acceptable precision. Equipped with these tools, theoretical predictions have served well on discovering unexplored properties and applications of the materials. Moreover, detailed characterizations at atomic scale benefits the experimental results as well, or even to explain the unexpected outcomes.

Considering all mentioned, it is a sound approach to apply state-of-the-art computational methods that accompanied with high-performance supercomputer facilities to investigate the physical properties of novel 2D materials. This thesis was initiated to this end and it is a summary of several works which has been accomplished during my PhD study. The thesis is organized as follows: For the rest of this chapter, I will first introduce graphene and some post-graphene materials that were discovered right after graphene and, briefly, several well-known methods used to synthesis 2D materials. The following chapter 2 will present the computational methods, the theory and the implementations of them in available software packages. In chapter 3, I will discuss several general

<sup>1</sup>Publication and patent results are obtained by searching for "graphene" in the topic field of Web of Science and the title field of PATENTSCOPE, respectively.

properties of 2D materials. The next two chapters will be the main results from my works. Starting from specific properties targeting specific novel 2D materials in ??, and followed by modification of physical properties of 2D materials in ?. Overlaps of materials themselves and their properties are inevitable between sections yet it will be minimized, such that each section will have a unique topic.

## 1.1 Graphene

Graphene is composed of carbon (C) atoms arranged on a honeycomb lattice in a single atomic layer. Graphite is made of van der Waals coupled graphene layers, see Fig. 1.2. These layers in graphite are stacked on top of another through weak physical bonds, whereas within each layer C atoms are hold together by strong chemical bonds. As a result, it is possible to just isolate a single layer from graphite without damaging the layer itself.

### 1.1.1 History

The story of graphene can be traced back to the discover of graphite around 1564 in England[5]. Ever since, people have been using graphite, the tip of a pencil, for writing and drawing. The black trace left behind by a pencil is actually stacks of graphite and graphene, but by chance even a single layer of graphene can be present. Apart from being a part of a pencil, graphite certainly has been holding a more important position in technology and industry due to its rich chemistry, low friction, high electrical and thermal conductivity etc. On the other hand, the synthesis of a single layer graphene seems to be discouraged by both experimental and theoretical limitation. On the experimental side, there have been attempts[6, 7, 8, 9] to isolate graphene from graphite or even grow it on a substrate. However, they were mostly failed due to the control of the number of layers and the difficulty to identify graphene itself. Addition to these experimental difficulties, theoretically, it was believed that strictly 2D materials should not exist due to a divergence in the thermal fluctuation in 2D materials that will make them unstable [10, 11, 12]. Nevertheless, graphene was still considered as a theoretical model. For example, Wallace [13] was the first to study the band

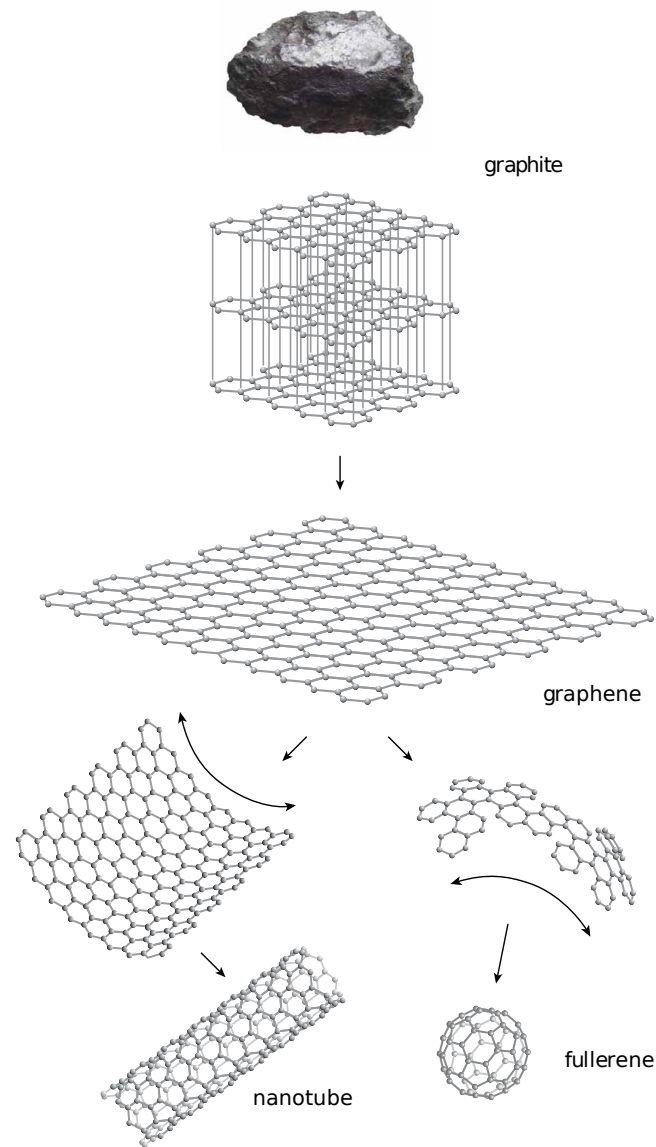


Fig. 1.2 Relation of graphite, graphene, fullerene and nanotube. Image source: the Nobel prize in physics 2010 [4].

structure of graphene [14] and found some of the interesting properties like a semimetallic band structure.

Although not in the form of graphene, the single atomic layer of graphite has been already seen and studied in other forms, e.g. fullerenes and nanotubes, see Fig. 1.2. These materials usually contain certain types of characteristic defects that make it different from graphite. Fullerene has a quasi-spherical hollow ball shape. It is composed of both six- and five-folded C rings, where the latter give positive curvature and made closed surface possible. The resulting shape resembles a football[15, 16]. The Nobel prize in chemistry of 1996 was award to Harold W. Kroto, Robert F. Curl and Richard E. Smalley for their discovery of fullerene. Another important type of carbon allotrope, carbon nanotubes[17], was discovered by using the arc-discharge method[16] which was originally designed to produce a large quantity of fullerenes. Despite sharing similar production method, carbon nanotubes are actually more close to graphene than fullerene due to the absence of pentagonal C rings in the former two. A carbon nanotube can be constructed by rolling up a graphene sheet into a hollow tube as its name suggest. Carbon nanotubes are observed to have micrometer in lengths and nanometer in diameter and having either metallic or semiconducting nature depending on the way they are rolled up. They possess superior mechanical properties. Individual nanotube has a Young's modulus of 0.64 TPa and it is 56 times stronger than steel wire[18].

In 2004, the situation has changed completely for graphene with the successfully isolation of a single layer of graphene from graphite by A. K. Geim and K. S. Novoselov at Manchester University using a simple micromechanical cleavage method. The key ingredient for success in this case as compared to the previous failures[6, 7], except for the sophisticated experimental control, is that the Si wafer under the graphene made it easier to identify graphene[3]. The synthesis of graphene itself already is a ground-breaking achievement, however, what excited the researcher the most is the extraordinary properties of graphene. In the following section, I will summarized some of them to illustrate this point.

### 1.1.2 Physical properties

As mentioned previously, graphene is a single atomic layer of graphite. It possesses an interesting structure with high symmetry which many of its properties are attributed to. Each C atom has three neighbours to which it is chemically bonded. Because of this, C atoms are arranged in a honeycomb lattice<sup>2</sup>, or a hexagonal Bravais lattice with two atoms per site, see (a) in Fig. 1.3. Graphene has uniform bond lengths of  $1.42\text{\AA}$  and uniform bond angles of  $120^\circ$ . The band structure which characterizes the electronic properties of graphene has been calculated by P. R. Wallace in 1947 [13]. He discovered that graphene is a semimetal with conduction band minimum (CBM) and valence band maximum (VBM) touch each other at the K and K' points in the first Brillouin zone as shown in (b) and (c) in Fig. 1.3. The energy-momentum dispersion is approximately linear in the vicinity of the K and K' points. Due to this, the electron and hole in those states behave differently as they do in a quadratic band. This has several consequences. First of all, considering the linear energy momentum relation, particles can be regarded as zero-mass Dirac particles and they are governed by relativistic Dirac equation[19], and they travel at constant speed of  $10^6\text{m/s}$ . Hence, the K and K' points are referred as Dirac points, their vicinities are called Dirac cones. Secondly, the carrier concentration can be tuned continuously from electron to hole with a perpendicular electric field[3]. Thirdly, the carrier in graphene can tunnel through a finite height potential if it normally incident without reflection — Klein tunnelling[20]. Fourthly, under a particular magnetic field, a zero energy Landau level appears, and the large energy interval between the zero and the first level made it possible to observe the quantum Hall effect at room temperature [21], etc.

Graphene delivers more than just interesting electronic properties. For example, evidencing the extraordinary mechanical properties, graphene has a Young modulus of  $1\text{Tpa}$  and intrinsic strength of  $130\text{ Gpa}$ [23]. This makes graphene the strongest material ever measured. More than 300 times stronger than steel and four times harder than diamond. Carrier high mobility is another exciting feature that has more applicative importance in electronic devices. Free standing graphene without substrate attached has been reported to have mobility of

---

<sup>2</sup>Honeycomb lattice is not a Bravais lattice.

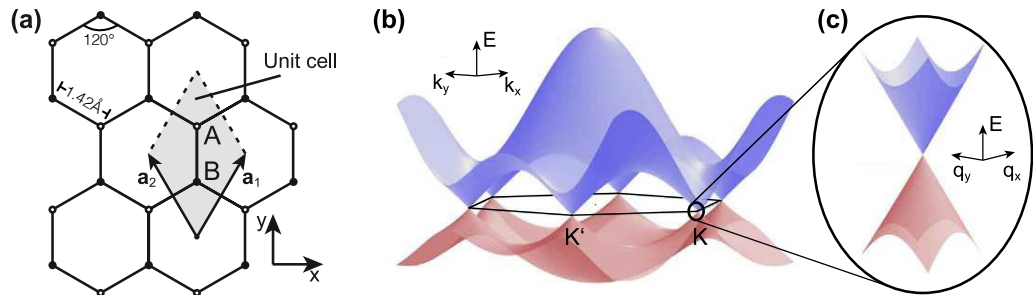


Fig. 1.3 (a) Graphene honeycomb lattice composed of A and B hexagonal Bravais sublattices. (b) Band structure of graphene where CBM and VBM touch each other only at the K and K' points. (c) Approximately linear dispersion around the K and K' points. Image source: [22].

230,000 cm<sup>2</sup>/Vs at low temperature[24] and 120,000 cm<sup>2</sup>/Vs at 240 Kelvin, the latter value is higher than that of any known semiconductor[25]. In addition, the thermal conductivity of graphene can reach up to 5000 W/mK at room temperature, which is 20 times higher than that of copper[26]. However, having a zero band gap means the application of graphene in digital logic gates is limited. The current controlled by the gate bias can not be turned off completely. Efforts to opening a band gap have been made, from substrate induction[27, 28], bi-layer graphene[29, 30], chemical adsorption[31, 32], and chemical doping[33] to quantum confinements[34, 35]. While doping and adsorption usually come with a cost of reducing mobility by introducing scattering centres, chemically pure bilayer graphene and nanoribbon are thought to be promising approaches to open a band gap as well as, to a great extend, preserve graphene's superior intrinsic properties.

## 1.2 Post-graphene materials and their general properties

Excitements of the exploration of graphene has driven the force to discover more types of 2D materials. Researchers have taken different approaches to this end. On the one hand, aiming to open a band gap in graphene, chemical functionalizations on graphene have been carried out with chemically adsorption of hydrogen, fluorine and oxygen, and resulting in graphane, fluorographene and

graphene oxide, respectively. On the other hand, inspired by graphite's layer structure, other layered materials are brought to the attention and efforts were undertaken to isolate single layer of it. In this section, I will introduce some of these early post-graphene materials and their physical properties in general.

### 1.2.1 Functionalized graphene

#### Graphane

The fully hydrogenation of graphene gives a 2-D hydrocarbon called graphane. It can synthesized either by reduction of graphite and then hydrogenation of left product (graphene, carbon nanotubes or graphite oxide) with liquid-based[36] or gas-based[37] environments, or growing by chemical vapour deposition[38].

Graphane is not flat as graphene. In fact, the bonding character changed from  $sp^2$  hybridization to  $sp^3$ , which results into buckled structure, see Fig. 1.4. Neighbouring H atoms locate at the different sides of the graphane plane. Among different phases of graphane, the chair structure was found to be the ground state. Others phases are metastable like: boat, twist-boat and twist-boat-chair[39]. The C-C bond length in the chair structure is 1.52 Å and thus larger than that in graphene. Graphane is a semiconductor with 3.5 eV band gap in the chair form. The band gap was reported to scale almost linearly with the hydrogen coverage[40]. The 2D Young's modulus of graphane is estimated 245 N/m[41] and thus smaller than 340 N/m of graphene. The incomplete coverage of H atoms on graphene gives hydrogenated graphene. It has a ferromagnetic magnetic state[42], tunable band gap[43] and reversible hydrogenation[31].

#### Fluorographene

More stronger binding between external atom and C atom can be realized using fluorine atom for adsorption. A full fluorinated graphene is called fluorographene, and it can be regarded as a single layer of graphite fluoride. Actually, sonochemical exfoliation of fluorographene from graphite fluoride is one of the ways to synthesis it, see Fig. 1.5[46]. Fluorographene has a similar structure as graphane due to the same  $sp^3$  hybridization, and it also has different isomers where the again the chair type is the ground state configuration[47]. The unit

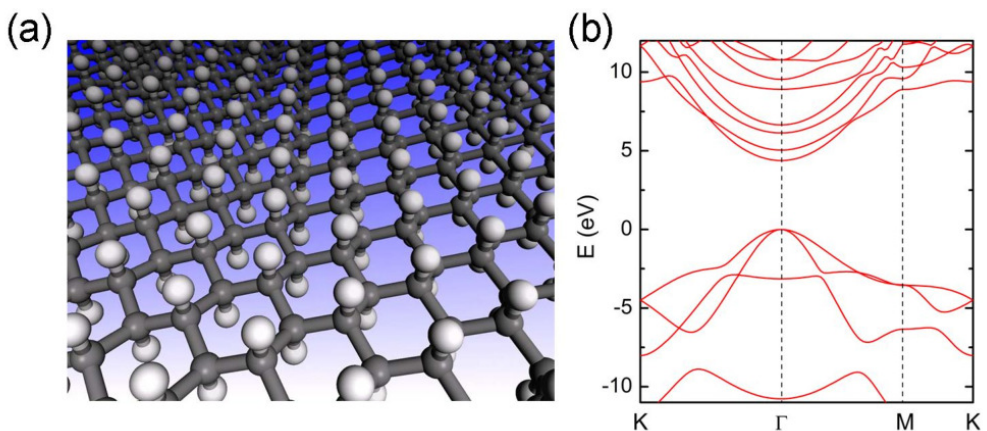


Fig. 1.4 (a)The chair structure of graphane. The white balls are the H atoms and the grey ones are the C atoms. Image source: [44]. (b) Band structure of chair graphane. Image source: [45]

cell of fluorographene is around 1% larger than that of graphene[48]. The formation energy of fluorographene is about 0.5 eV per fluorine atom lower than that of graphane per hydrogen atom[32]. The band gap of fluorographene is larger than 3 eV from optical measurement[48, 32], and the band structure is similar to that of graphane with a band gap at the  $\Gamma$  k-point. The 2D Young's modulus of fluorographene is 100 N/m and the intrinsic strength is about 15 N/m. Both are more than two times less than those for graphene due to the weaker sp<sup>3</sup> bonds in fluorographene[48].



Fig. 1.5 Graphite fluoride to fluorographene. Image source:[46]

### 1.2.2 Group IV 2D materials

Analogues to graphene, 2D materials made of only single elements from other members of group IV have been also proposed and synthesized. These are silicene, germanene, stanene which are made of silicon (Si), germanium (Ge) and tin (Sn) atoms, respectively. They generally suffer from less stability as compared with graphene. The free standing form of these materials are hard to make, instead they usually need ordered substrates to support them. Therefore, measurements done on these type of systems are thought not necessarily representative for the target material, the influence of the substrate is not negligible[49]. This will in turn hinder the accurate determination of their properties. Despite these experimental difficulties, theoretical studies have more freedom to investigate their physical properties. One of the most important differences of these materials as compared to graphene is their not-flat buckled structure, see Fig. 1.6. The buckling parameters  $\delta$  is defined as the interlayer distance of layers at different 2D atomic planes. According to calculations,  $\delta$  is 0.45 Å for silicene, 0.69 Å for germanene and 0.85 Å for stanene[50]. This change corresponds to a more  $sp^3$  character in the orbitals, and it increases with the atomic radius.

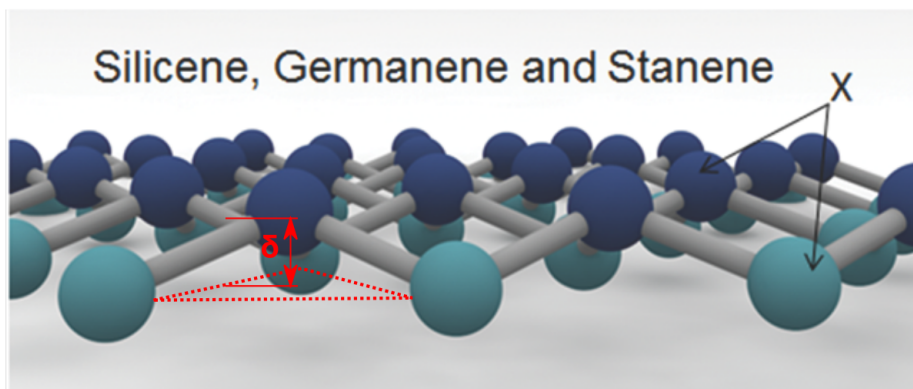


Fig. 1.6 Buckled hexagonal crystal structures of 2D group IV materials ( $X = Si, Ge,$  and  $Sn$ ). Different colors represent different 2D planes and their distance is the buckling parameter  $\delta$ . Image adapted from:[51]

Although having a buckled structure, these materials also posses Dirac points with linear energy momentum dispersion around it[52]. However, as stated before, the substrate that supports these materials will induce symmetry breaking which leads to the lost of the Dirac character of the electrons/holes[49]. More-

over, spin-orbit coupling (SOC) in these materials are predicted to be larger than that in graphene due to larger atomic weights. With inclusion of SOC, this corresponds to 1.9 meV band gap in silicene and 101 meV of that in stanene[50]. The mechanical stiffness and strength are low as compared to graphene and has a reducing trend with increasing atomic number in this group. This is partially due to the less energetically costly bond angle deformation in the buckled structure upon load rather than bond stretching in a flat structure[53]. For example, silicene has a 2D Young's modulus around 62 N/m, that is four times smaller than graphene. Another important difference of these materials from graphene regards the realization of a monolayer. The lack of layered bulk materials for the former ones made the mechanical exfoliation inapplicable for them, which is believed to produce the highest quality sample otherwise. Therefore, methods used in this case are either bottom-up decomposition techniques onto highly ordered substrates[54, 55], or top-down methods like chemical exfoliation to isolate grown monolayer from substrate[56, 57].

### 1.2.3 2D from layered materials

The layered structure of graphite contribute the most to the isolation of graphene. If the interlayer bonding were not the weak vdW interaction but rather a covalent type, even the concept of layers can not stand let alone to break the bonds only in one direction and keep others in the other two directions. Therefore, a reasonable way to explore other 2D materials is through other layered materials, e.g. hexagonal boron nitrides, transition metal dichalcogenides. In this section, I will discuss the general physical properties of these two materials as examples for 2D materials from layered materials.

#### Boron Nitride

Among the multiple structural phases of Boron Nitride, the layered hexagonal phase (h-BN) is the most stable one, see Fig. 1.7 for the structure. A single layer extracted from it gives 2D h-BN. Because of its structural similarity to graphene and its wide band gap it is often referred as white graphene[58]. 2D h-BN has a band gap of 6.1 eV according to calculations. A intuitive tight binding analysis reveals the band gap, in the case of 2D h-BN, to be proportional to the difference

of  $p_z$  orbitals from B and N atoms. For silicene and graphene, this difference is zero thus so is the band gap. Moreover, as a result of different electronegativity, i.e. 2.0 for B and 3.0 for N, ionic character develops which further enlarges the band gap[59]. Several interesting features of this material are reported: strong mechanical stiffness and strength close to graphene[60], a good thermal conductivity of  $100\text{-}270 \text{ W m}^{-1} \text{ K}^{-1}$  for few-layer h-BN[61] as an electrical insulator, a high oxidation resistance up to  $700^\circ\text{C}$  in contrast to  $400^\circ\text{C}$  for graphene[62], etc.. Benefit from its compatible bond length, i.e. 1. Å, with graphene, it is a perfect partner for graphene to form heterostructure electronic devices to serve as a dielectric substrate[63], resulting in larger mobility for graphene as compared to  $\text{SiO}_2$  substrate[64] for instance.

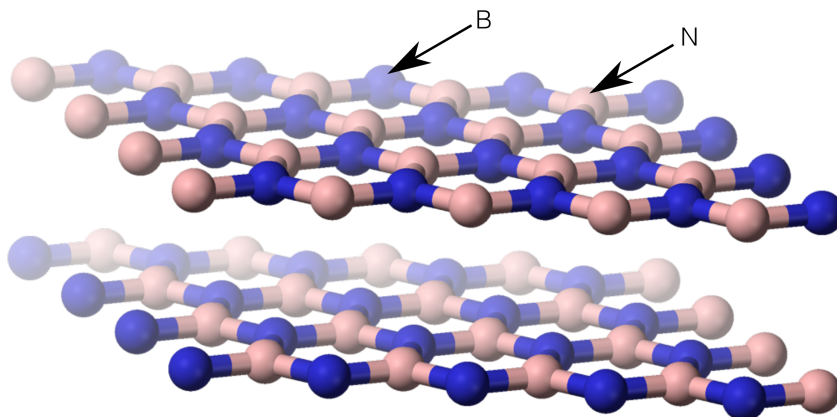


Fig. 1.7 Layered hexagonal crystal structures of h-BN. Image adapted from:[65]

### Transition Metal Dichalcogenides

Transition metal dichalcogenides (TMDs) have a general formula of  $\text{MX}_2$ , where M stands for the group 4-7 elements in the transition metal series in the periodic table, and X are the group VI elements. This is another type of layered materials, and the single layer of some of them have been experimentally realized. These materials typically exist in three different structural phases as shown in Fig. 1.8, which at monolayer level can be either H or T phase. One of the most important differences in these two phases is the lack of inversion symmetry in H phase in contrast to the T phase. Therefore, spin orbit coupling (SOC) is more important in

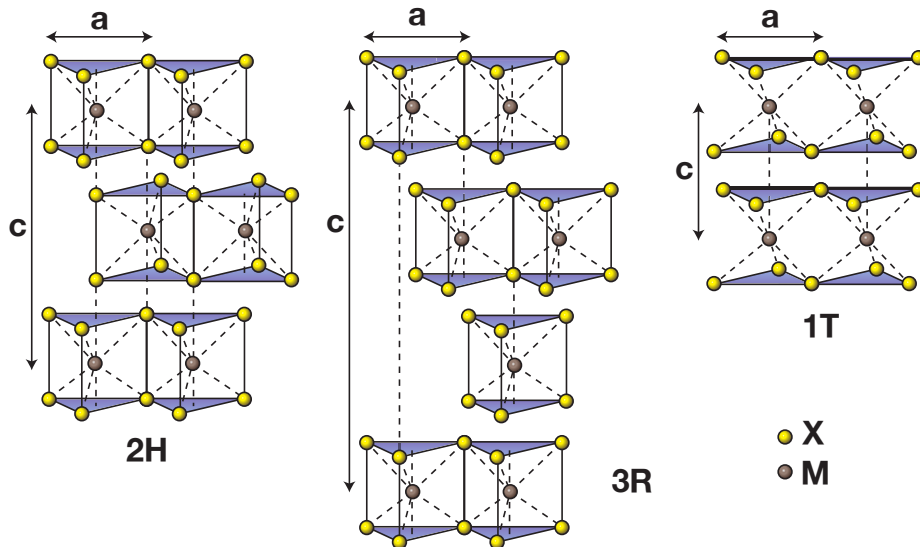


Fig. 1.8 Layered structures of TMDs. 2H: two layers per unit cell with hexagonal symmetry; 3R: three layers per unit cell with rhombohedral symmetry; 1T: one layer per unit cell with tetragonal symmetry.  $a$  is the in-plane lattice constant with a range from 3.1 to 3.7 Å in TMDs.  $c$  is the vertical lattice constant. The interlayer distance has a typical length of 6.5 Å. Image source: [66]

H and induces spin-splitting, for instance 456 meV electron spin states splitting in WSe<sub>2</sub>[67] has been reported. Note that, inversion symmetry is recovered in the layered bulk form hence suppresses SOC. Another important consequence of reduce dimensionality is the indirect-to-direct band gap transition from layered TMDs to its 2D counterpart, see for example Fig. 1.9. 2D-TMDs have a broad range of potential applications. Electrocatalysis[68, 69] benefit from adequate active sites, electronic devices[70, 71] benefit from typical band gap of 1-2 eV, Li or Na batteries[72, 73] benefit from high surface-to-volume ratio and short diffusion path, photocatalysis benefit from high stability under extreme light intensity[74, 75], and biomedicine benefit from enhancement of the physiological stability and biocompatibility of polymers on 2D-TMDs[76, 77].

### 1.3 1D from 2D: nanotubes and nanoribbons

The reduction of dimensionality of the materials did not stop at the 2D level. Further lowing it will result in 1D nanotubes or nanoribbons. A nanoribbon is

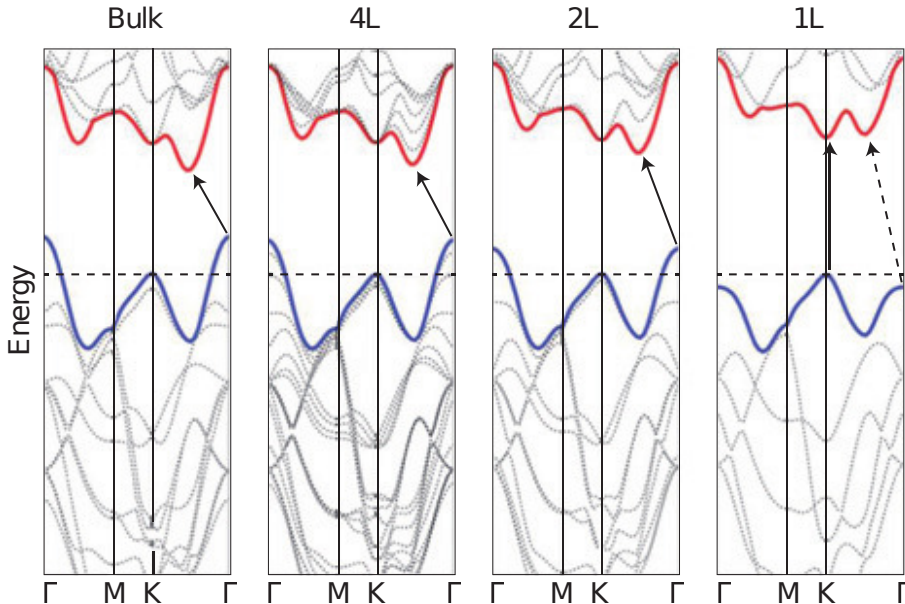


Fig. 1.9 Band structure evolution of MoS<sub>2</sub> from bulk to single layer. Image source: [78]

a strip of 2D sheet with nano-scale width and micro-scale length and it is still flat. Whereas nanotubes are the rolling up of nanoribbons resulting in a tube structure. Each nanotube, also each nanoribbon but with different definition, is associated with a chiral vector that uniquely defines its structure parameters expect the length which is consider to be infinite in theory. In Fig. 1.10,  $\vec{a}_1$  and  $\vec{a}_2$  are the unit lattice vectors in graphene. Chiral vector,  $\vec{C}$ , is the superposition of these two unit vectors with indices pair  $(n,m)$ . Zigzag edge always has a  $(n,0)$  form and  $(n,n)$  is always armchair edge. Everything else is called chiral type edge. This finite-length chiral vector also defines the radius of the tube. Nanoribbons, on the other hand, have these three types of edges as well. However, in this case, edges have infinite length.

With confinements from other directions, physical properties of these systems are expected to be different than that for their higher dimension counterparts. For example, graphene nanoribbons have a finite band gap in contrast to the zero band gap of graphene[79]. Moreover, control of this confinement will give tunable physical properties. For example, overall inverse band gap relation with the width of the nanoribbon[80]. The zigzag edges in graphene

nanoribbon form spin-polarized magnetic states and give ferromagnetic ordering along the edge and anti-ferromagnetic ordering across edges[81]. For nanotubes, those having the same edges belong to the same class of chirality and have the same electronic structure. For instance, armchair carbon nanotubes are metallic, other types are semiconducting. But small radius tubes can be exceptional due to the large curvature[82]. The strong mechanical strength and high thermal conductivity of a graphene nanoribbon is similar to those in graphene.

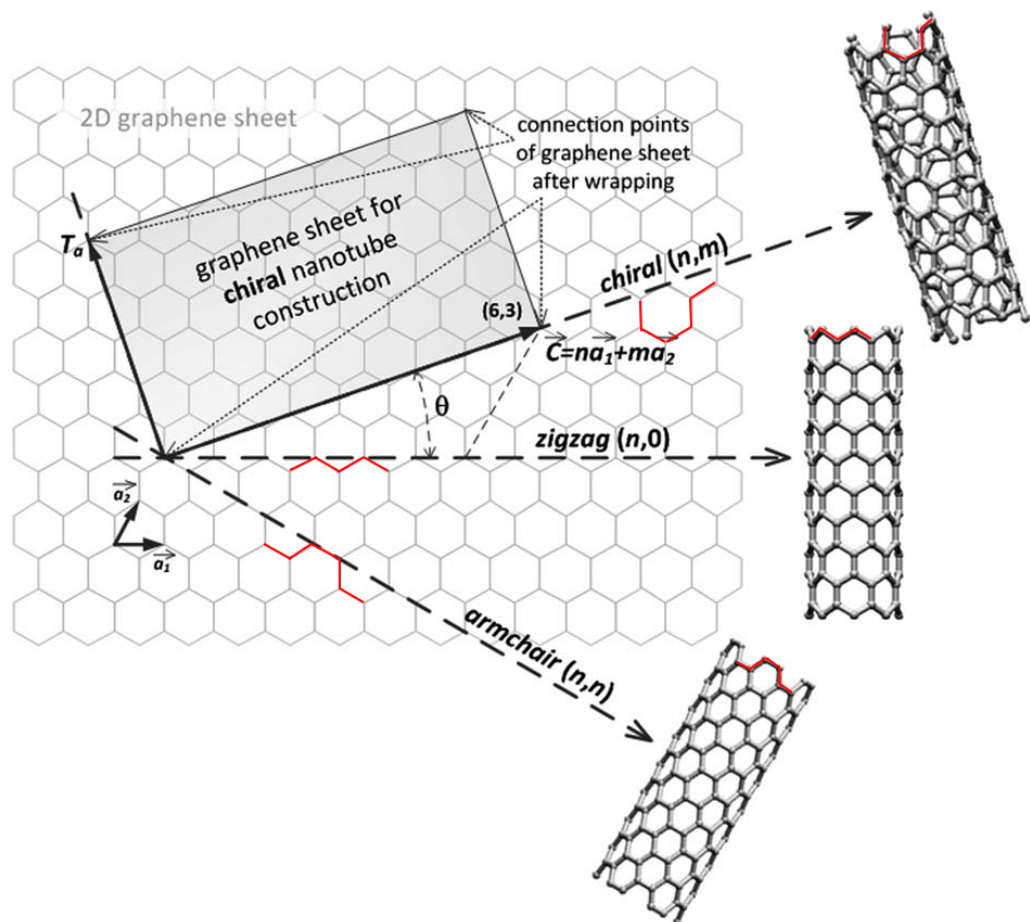


Fig. 1.10 Chiral vector and different type of nanotubes as obtained by rolling them up in different directions. Image adapted from [83]

## 1.4 Synthesis methods

In this last section, I will briefly discuss some of the well-known synthesis methods for 2D materials. In Fig. 1.11, an overview of graphene production methods is displayed in Fig. 1.11.

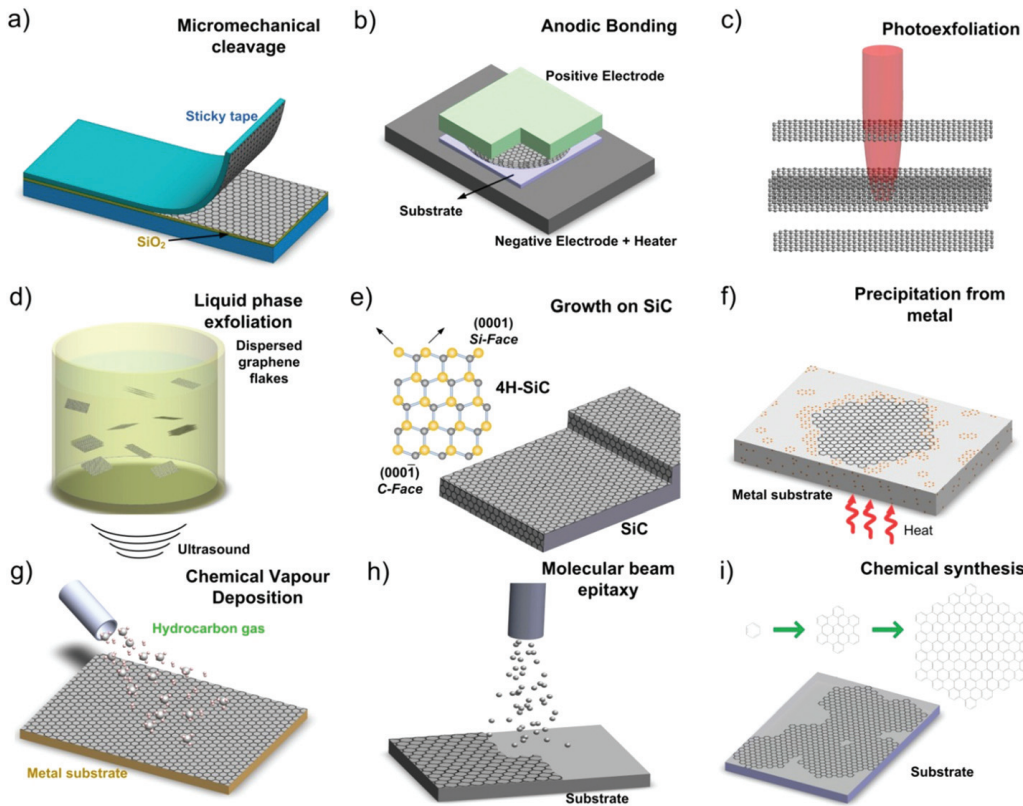


Fig. 1.11 Graphene production setups. Image source [84]

### Micromechanical cleavage

Micromechanical cleavage is also known as mechanical exfoliation, which was the method used to first successful isolation of graphene in 2004 using an adhesive tape[2]. It involves separating layers in layered materials by mechanical, electrostatic, or electromagnetic forces. This method gives high quality product and is suitable for laboratory-scale sample ideal for fundamental studies. Large scale productions are impractical through this method. Room temperature mo-

bility was measured up to  $20,000 \text{ cm}^2\text{V}^{-1}\text{s}^{-1}$ [85] on graphene prepared with this method.

### Liquid phase exfoliation

Liquid phase exfoliation is the extraction of layers in a proper solvent using ultra-sounds. The cavitation-induced bubbles collapse around the graphite will generate a compressive stress wave. As a primary result, this will cause a reflective tensile wave whose strength is proportional with the number of such bubbles. Intensive tensile stress is enough to break graphite into graphite flakes. Additionally, as a secondary effect, shear effect can be developed from unbalance lateral stress, and separate two adjacent layers. Liquid phase exfoliation is a promising method to synthesis cheap and scalable samples.

### Growth on SiC

Growth of graphene on SiC involves SiC sample annealing at high temperature ( $> 1400^\circ\text{C}$ ) in vacuum or under atmospheric pressure. The sublimation of silicon atoms leave behind carbon atoms on the surface which will rearrange to form a graphitic layer[86], see Fig. 1.12. Apart from high reproducibility and production of homogeneous large-area sample by this method, it has the advantage that graphene is available on a semiconducting substrate for layer electronic device integration.

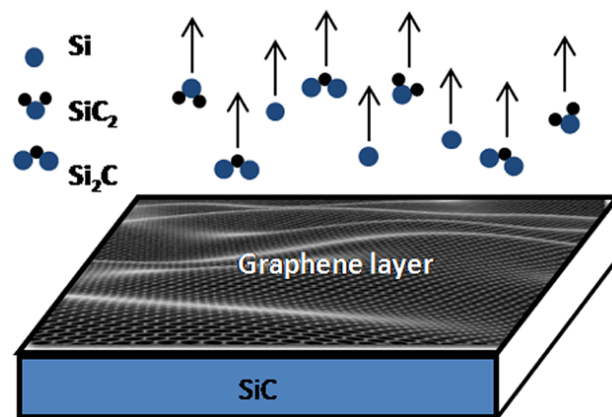


Fig. 1.12 Growth of graphene on SiC wafer. Image source [87]

### Chemical vapor deposition

Chemical vapor deposition (CVD) is a popular method to grow amorphous or crystalline thin film from solid, gaseous or liquid precursors. It is a direct deposition of vaporized desired material onto a particular substrate. Various CVD methods exist depending on their operating pressure, types of vaporization and whether it is plasma-assisted etc.. Graphene grown on transition metals usually is of high quality. Carbon atoms from organic sources in the gas phase are deposited on a metal (Ni, Ru, Ir etc.) and convert to graphene at high temperature. Then, for the characterization, graphene is transferred to a proper substrate. Typical mobility of such type of sample is around  $1000\text{-}25000 \text{ cm}^2\text{V}^{-1}\text{s}^{-1}$ [88]. A 30-inch graphene film has been produced from roll-to-roll production through CVD methods by Bae et al. [89], see Fig. 1.13. The measured product was found to be a better electrode than commercially available indium tin oxides.

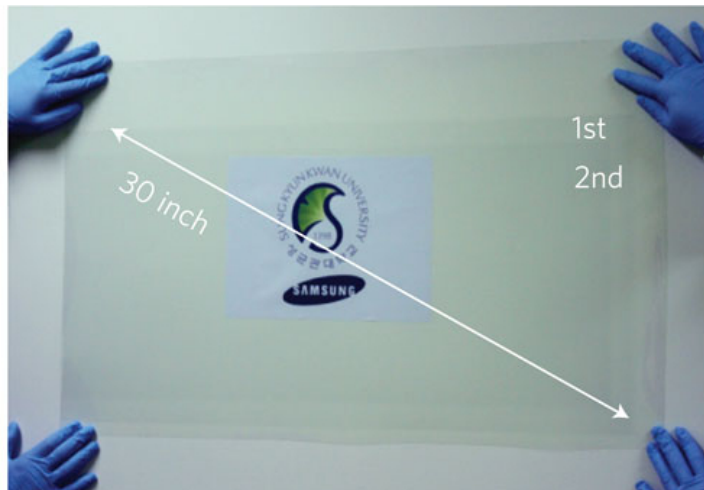


Fig. 1.13 A ultra-large-area graphene film. Image source [89]

# **Chapter 2**

## **Computational methods**

Theories behind the calculations are the core component in the material properties determination process. Its correctness, accuracy and implementation directly influence the quality of its predictions. In this chapter, I will introduce relevant theoretical models, approximations and their implementations in commonly used software packages.

### **2.1 Theory**

#### **2.1.1 Density Functional Theory**

Density functional theory (DFT) is one of the most widely used quantum mechanical method to calculate the properties of materials. Its applicable length and time scale are in nanometre and picoseconds, respectively. These scales are longer than for quantum Monte Carlo simulations, but lower than for semi- or full-empirical methods in both scales. This is also so in the accuracy verse size-of-the-system plot in Fig. 2.1. The accuracy of different methods can be higher than that in the plot, since a large part of the inaccuracy can be attributed to the uncertainty of the experimental results that the methods are compared with[90]. As I will discuss in the later section, if a DFT method is compared with a highly accurate theoretical benchmark method, DFT would have a precision around 1 meV/atom. For bulk or nanostructures, DFT can be used to even quantitatively predict the properties of materials. DFT is based on: Hohenberg-Kohn theorems[91] and Kohn-Sham equations[92]. Here I will briefly overview these

without putting too much stress on the derivation which have been extensively documented in textbooks. Materials are made from electrons and nuclei. Type

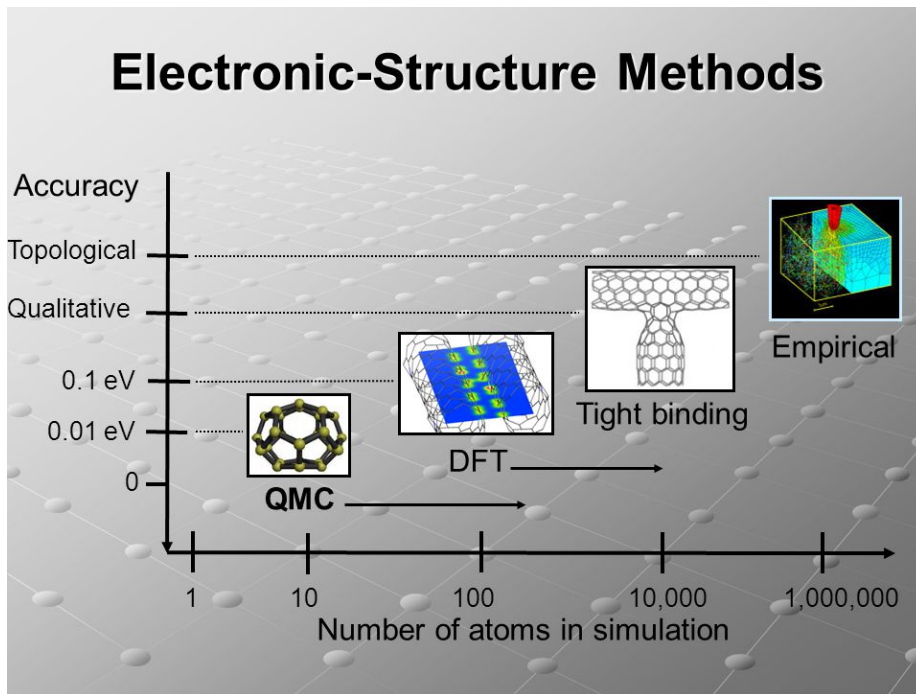


Fig. 2.1 Comparison of the accuracy and the size of electronic structure calculation methods. Image source: [93].

of nuclei and the interactions between these components give rise to various materials and their properties. The interactions are mainly electrostatic or Coulombic. While electrons must be described with quantum mechanics, the nuclei can be treated as classical particles. The equation governing electron behaviour is

the Schrödinger equation. It can be written as follows:<sup>1</sup>

$$\begin{aligned}
 \hat{H}\psi_\alpha(\vec{r}_1\sigma_1, \dots, \vec{r}_N\sigma_N) &= \left[ -\frac{1}{2} \sum_{i=1}^N \nabla_i^2 + \sum_{i=1}^N v(\vec{r}_i) + \frac{1}{2} \sum_{i=1} \sum_{j \neq i} \frac{1}{|\vec{r}_i - \vec{r}_j|} \right] \psi_\alpha(\vec{r}_1\sigma_1, \dots, \vec{r}_N\sigma_N) \\
 &= (\hat{T} + \hat{V}_{ext} + \hat{V}_{ee}) \psi_\alpha(\vec{r}_1\sigma_1, \dots, \vec{r}_N\sigma_N) \\
 &= E_\alpha \psi_\alpha(\vec{r}_1\sigma_1, \dots, \vec{r}_N\sigma_N).
 \end{aligned} \tag{2.1}$$

$\hat{H}$  is the total Hamiltonian,  $\hat{T}$  is the kinetic energy,  $\hat{V}_{ext}$  is the interaction between electrons and nuclei. Here we already started with the first approximation: Born–Oppenheimer approximation[94]. Which neglect the dynamics of nuclei and electrons are considered moving in a static potential generated by their interaction with all nuclei.  $\hat{V}_{ee}$  is the interaction between electrons. The first two terms sum over all  $N$ -electrons, and the last one sums over all pairs of  $N$ -electrons.  $\vec{r}$  is the electron position,  $\sigma$  is the z-component of the spin of an electron ( $+\frac{1}{2}, -\frac{1}{2}$ ).  $\psi$  is the  $N$ -electron wave function, which should be antisymmetric under interchange of the orbital and spin coordinates of two electrons (i.e. fermionic character for electrons) and it should also satisfy the boundary condition of the system (e.g. quantum confinement for low-dimensional system).  $E$  is the total energy, and  $\alpha$  is the complete set of  $N$ -electron quantum numbers.

Following the constrained search algorithm introduced by M. Levy[95], the ground-state energy  $E$  can be found by minimizing the expectation value of the total Hamiltonian with respect to wave function:

$$E = \min_{\psi} \langle \psi | \hat{H} | \psi \rangle. \tag{2.2}$$

Here we take two steps for the minimization. For the first step, we minimize with respect to all wave functions that give the same density  $n(\vec{r})$ :

$$E = \min_{\psi \rightarrow n} \langle \psi | \hat{T} + \hat{V}_{ee} | \psi \rangle + \int d\vec{r}^3 v(\vec{r}) n(\vec{r}). \tag{2.3}$$

---

<sup>1</sup>Equations in this chapter are written in cgs form: length, mass, time and energy are in the units of centimetre, gram, second and erg, respectively. Additionally, fundamental constants  $\hbar$ ,  $e^2$  and  $m$  are set to unity.

Then with the resulting wave function  $\psi_n^{min}$  that yields the minimum energy  $E$  associated with the density  $n(\vec{r})$ , we can construct the universal functional:

$$\min_{\psi \rightarrow n} \langle \psi | \hat{T} + \hat{V}_{ee} | \psi \rangle = \langle \psi_n^{min} | \hat{T} + \hat{V}_{ee} | \psi_n^{min} \rangle = F[n(\vec{r})]. \quad (2.4)$$

From this equation, we see that the functional,  $F[n(\vec{r})]$ , is a function of a function. For the second step, we minimized with respect to all densities  $n(\vec{r})$ :

$$E = \min_n \left\{ F[n(\vec{r})] + \int d\vec{r}^3 v(\vec{r}) n(\vec{r}) \right\}, \quad (2.5)$$

where  $v(\vec{r})$  is kept fixed during the minimization. The resulting density is the ground-state density that gives the lowest ground state energy. This is known as the density variational principle, also the main idea of the Hohenberg-Kohn theorems. For the completeness, the theorems are present in the following:

**Theorem 1** *The external potential,  $V_{ext}(\vec{r})$ , of any system of interacting particles is uniquely determined (up to a constant) by the particle density,  $n_0(\vec{r})$ , of the ground state.*

**Theorem 2** *The ground state energy of a system with an external potential  $V_{ext}(\vec{r})$  is given by the minimum value of the energy functional  $E_{HK}[n]$  and the density for which this minimum is reached corresponds with the ground state density  $n_0(\vec{r})$ .*

Now, the main problem is to define the approximated expression of  $F[n(\vec{r})]$ . Kohn-Sham equation is a elegant way to do this. It aims to construct a non-interacting system, where kinetic energy can be calculated exactly, where the local external potential  $V_{KS}(\vec{r})$  is added. The  $F[n]$  decomposes into the following, where  $E_{XC}[n]$  is the exchange-correlation (XC) energy:

$$F[n] = T_s[n] + E_H[n] + E_{XC}[n], \quad (2.6)$$

where  $T_s[n]$  is the non-interacting kinetic energy functional, and  $E_H[n]$  is the Hartree energy functional:

$$E_H[n] = \frac{1}{2} \int d^3 r \int d^3 r' \frac{n(\vec{r})n(\vec{r}')}{|\vec{r} - \vec{r}'|}. \quad (2.7)$$

Apart from the last term,  $E_{XC}[n]$ , everything else can be exactly calculated for non-interacting system for given density. By imposing a normalisation constraint on the electron density,  $\int n(\vec{r})d\vec{r} = N$ , we have

$$\frac{\delta F[n]}{\delta n(\vec{r})} = -v(\vec{r}). \quad (2.8)$$

Therefore, the effective local potential,  $V_{KS}(\vec{r})$ , will be

$$V_{KS}(\vec{r}) = v(\vec{r}) + \frac{\delta E_H[n]}{\delta n(\vec{r})} + \frac{\delta E_{XC}[n]}{\delta n(\vec{r})}, \quad (2.9)$$

and the Kohn-Sham equation reads

$$\left[ -\frac{1}{2}\nabla_i^2 + v(\vec{r}) + \frac{\delta E_H[n]}{\delta n(\vec{r})} + \frac{\delta E_{XC}[n]}{\delta n(\vec{r})} \right] \psi_\alpha(\vec{r}\sigma) = \epsilon_\alpha \psi_\alpha(\vec{r}\sigma), \quad (2.10)$$

and ground-state density is

$$n(\vec{r}) = \sum_{\alpha}^{occ.} \sum_{\sigma} |\psi_\alpha(\vec{r}\sigma)|^2. \quad (2.11)$$

This can be solved self-consistently. An initial guess on the density  $n(\vec{r})$  determines the effective potential  $V_{KS}(\vec{r})$ , from equation (2.10) wave functions  $\psi_\alpha(\vec{r}\sigma)$  can be calculated, which will give a new density through equation (2.11). This procedure is repeated until self-consistency is reached.

### 2.1.2 Exchange-correlation functional

The XC energy functional is not known exactly and therefore needs to be approximated. The choice of it directly influences the accuracy of the results. This is because, although it is often a small fraction of the total energy, its contribution to the chemical bonding and the formation energy is relatively important. The generalized gradient approximation (GGA) has become popular in solid state calculations. It is a further upgrade of its previous version, the local density approximation (LDA). The LDA has the following form:

$$E_{XC}^{LDA}[n] = \int n(\vec{r}) \epsilon_{XC}[n(\vec{r})] d\vec{r}. \quad (2.12)$$

$\epsilon_{XC}[n(\vec{r})]$  is the XC energy for an homogeneous electron gas having density  $n$ , and it is usually taken from quantum Monte Carlo calculations. Whereas the GGA further includes the derivative of density,  $\nabla n(\vec{r})$ , as an argument for  $\epsilon_{XC}$ , thus it reads

$$E_{XC}^{GGA}[n] = \int \epsilon_{XC}[n(\vec{r}), \nabla n(\vec{r})] d\vec{r}. \quad (2.13)$$

In contrast to LDA, there is no unique input for  $\epsilon_{XC}[n(\vec{r}), \nabla n(\vec{r})]$ . Different constructions for GGA usually named with the corresponding authors, e.g. PW91-GGA stands for Perdew and Wang's GGA construction in 1991[96, 97] and PBE-GGA stands for Perdew, Burke, and Ernzerhof [98]'s construction. They are the most popular GGA approximations for solid state systems.

### Jacob's ladder

Jacob's ladder is a ladder connecting earth and heaven that biblical Patriarch Jacob dreamed about. Professor John P. Perdew, who is known for profound contribution to DFT and XC functionals, used it analogously to describe the hierarchy of density functional approximations in terms of their accuracies, see Fig. 2.2. Each rung is a level of approximation constructed with different formalisms. From LDA and GGA as mentioned to meta-GGA which includes the Kohn-Sham kinetic energy density. Next higher in the ladder is the hybrid functionals which incorporates a part of the exact exchange from Hartree-Fock (HF) theory. For example, the PBE0 functional[100] has the following definition:

$$E_{XC}^{PBE0} = \frac{1}{4} E_X^{HF} + \frac{3}{4} E_X^{PBE} + E_C^{PBE}, \quad (2.14)$$

and the HSE06 (Heyd-Scuseria-Ernzerhof)[101] take into account the screened Coulomb potential for the exact part:

$$E_{XC}^{HSE} = \beta E_X^{HF,SR}(\omega) + (1 - \beta) E_X^{PBE,SR}(\omega) + E_X^{PBE,LR}(\omega) + E_C^{PBE}, \quad (2.15)$$

where  $\beta$  is the mixing parameter and  $\omega$  is the parameter to control the screening range which defines the short-range, SR, and long-range, LR, parts. The values of  $\beta = 1/4$  and  $\omega = 0.2$  corresponding to HSE06 functional which gives accurate band gaps and lattice constants, see the Mean absolute error (MAE) of different functionals in Fig. 2.3. The highest ranked functionals are the double hybrid

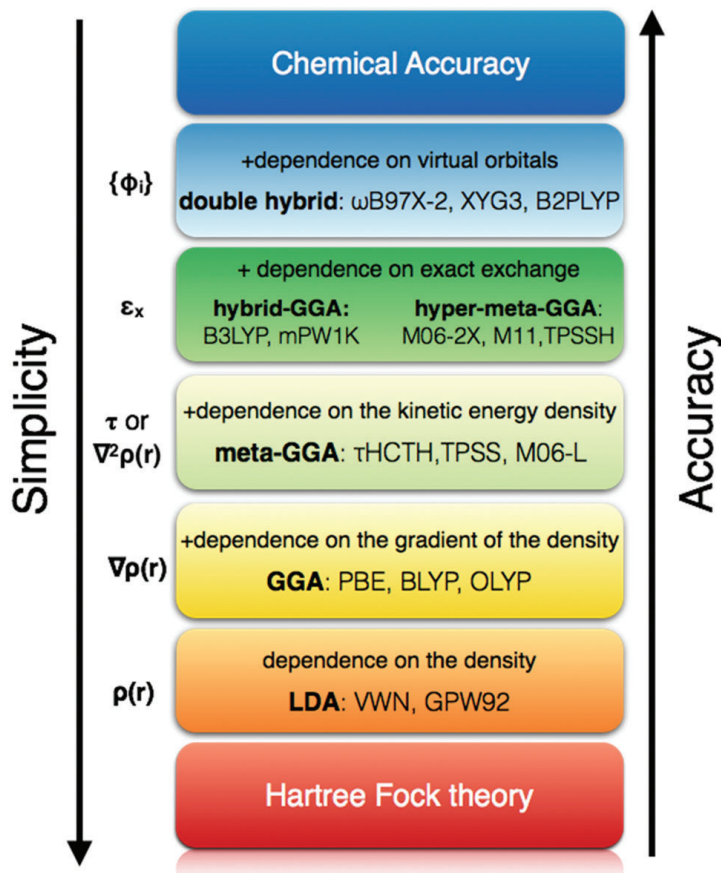


Fig. 2.2 Jacob's ladder for DFT approximations. Image source: [99].

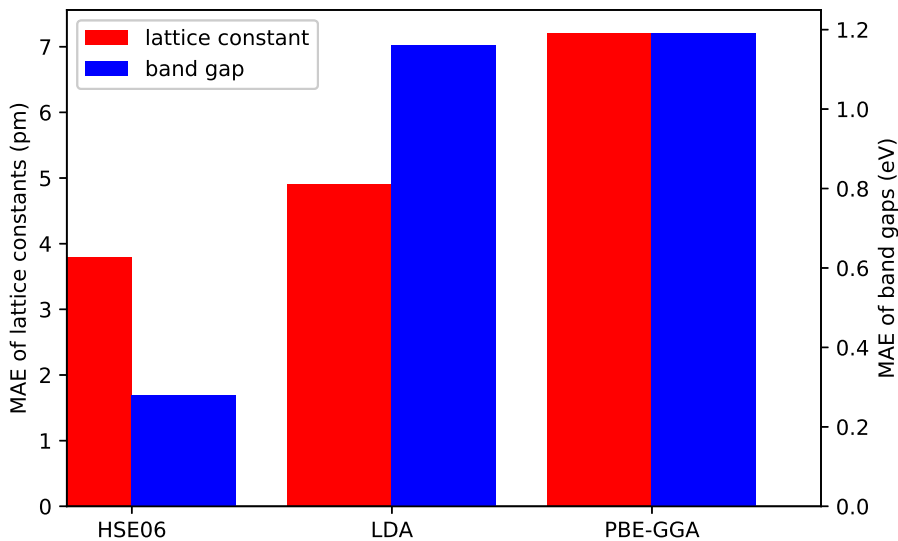


Fig. 2.3 MAE of the equilibrium lattice constants and band gaps of different functionals on SC40 solid test set<sup>1</sup>. Data source: [102].

which includes the unoccupied orbitals as well, e.g. Random Phase Approximation[103].

### Band gap problem

As shown in Fig. 2.3, band gap estimation in LDA and GGA is quite poor. This can be attributed to the highly non-analytical and non-local behaviours of the XC energy functional. In other words, it means the energy increase by adding an extra electron in the extended system is of the order of 1 eV, even though, it is an infinitesimal density change. Let's look at the definition of the band gap  $E_g$ :

$$E_g = I - A = \epsilon_{N+1}^{KS,HOMO} - \epsilon_N^{KS,HOMO}, \quad (2.16)$$

where  $I$  is the ionization energy, the energy change by removing one valence electron;  $A$  is the electron affinity, the energy change by adding one electron to a neutral system;  $\epsilon_N^{KS}$  Kohn-Sham orbital energy for  $N$ -electron system, and  $HOMO$  stand for the highest occupied molecular orbital; The  $LUMO$  below

---

<sup>1</sup>The SC40 test set is a collections of 40 elementary and binary solid compounds of various structures with a wide range of band gaps

stands for the lowest unoccupied molecular orbital. For a non-interacting Kohn-Sham system,  $E_g^{KS}$  can be calculated as follows:

$$E_g^{KS} = \epsilon_N^{KS,LUMO} - \epsilon_N^{KS,HOMO}. \quad (2.17)$$

This leads to

$$E_g = E_g^{KS} + \Delta_{XC}, \quad (2.18)$$

where  $\Delta_{XC}$  is the orbital shift caused by adding an extra electron:  $\epsilon_{N+1}^{KS,HOMO} - \epsilon_N^{KS,LUMO}$ . The  $\Delta_{XC}$  exclusively depends on the non-analyticity of the XC potential.

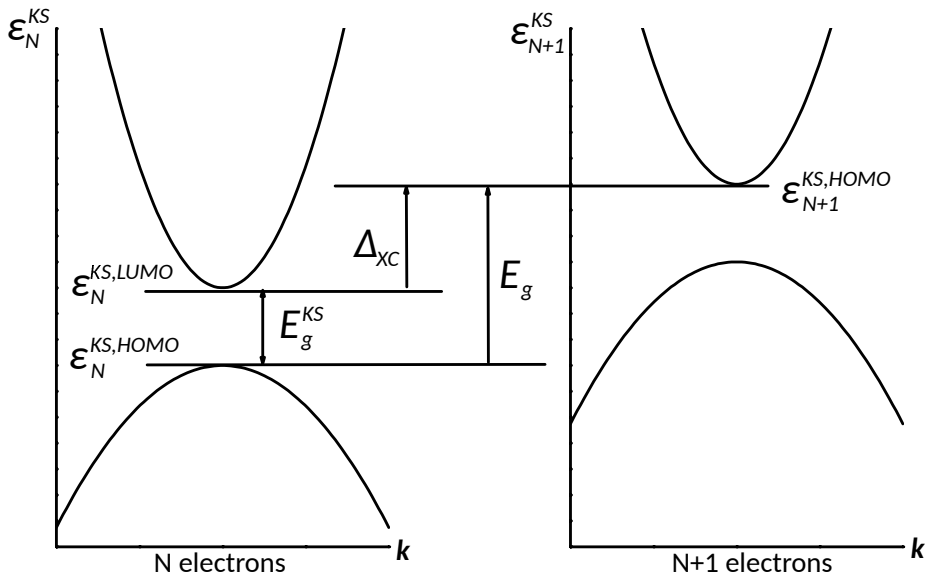


Fig. 2.4 Schematic illustration of the relation between  $E_g$  and  $E_g^{KS}$ . Image adapted from: [104].

tial  $\frac{\delta E_{XC}[n]}{\delta n(\vec{r})}$ , since the Hartree potential explicitly depends on the density. If the XC energy functional were analytic, the infinitesimal density variation would not introduce a large potential change, hence  $\Delta_{XC}$  is small or equals to zero, and  $E_g \approx E_g^{KS}$ . The band gap accuracy when compared with experiment would be only limited inherently by different functionals. However, non-zero  $\Delta_{XC}$  has been reported on many materials and it is responsible for 80% of the LDA band gap error[105].

## 2.2 Implementation

The implementations of the theory in the last section are crucial and not always straightforward. Many of the quantities are represented with technically easily implemented functions, and they have to be finite in size or quantity. Question rises on how much would be enough? This is equivalent to the computational convergence. Here we review two of the most important convergence parameters:  $\mathbf{k}$  points and cut-off energy of the basis set.

### $\mathbf{k}$ points

According to Bloch's theorem, the solution of the Schrödinger equation for a periodic system, e.g. a crystal with a well-defined unit cell, can be expressed through the following:

$$\phi_{\mathbf{k}}(\mathbf{r}) = e^{i\mathbf{k} \cdot \mathbf{r}} u_{\mathbf{k}}(\mathbf{r}), \quad (2.19)$$

where  $\phi$  is the wave function,  $u$  is a function having the same periodicity as the crystal. The space of vector  $\mathbf{r}$  and  $\mathbf{k}$  are called real and reciprocal space ( $\mathbf{k}$  space), respectively. Particularly, each point in  $\mathbf{k}$  space is associated with an unique  $\mathbf{k}$  vector and is usually called a  $\mathbf{k}$  point. Making use of the symmetry of the system, all inequivalent  $\mathbf{k}$  points reside inside a finite sub-space of  $\mathbf{k}$  space, called the first Brillouin zone (FBZ). Quantity evaluations are mostly done through the integration of wave functions, or other functions have  $\mathbf{k}$  dependence, over the FBZ. This integration has to be done numerically since explicit relation of  $\phi$  and  $\mathbf{k}$  is unknown. In practice, the FBZ is discretized into a grid defined by the mesh of the  $\mathbf{k}$ -points. This mesh has to be large for accurate sampling of FBZ yet it should be small for less computational time and resource. This is one of the convergence tests that needs to be done in order to obtain reliable results. Usually, metals need more  $\mathbf{k}$ -points than semiconductors. This is because the highest occupied valence band crosses the Fermi energy in metals, hence the integration for all occupied states is done for a discontinuous function that excludes unoccupied states. Whereas for a semiconductor or insulator, the highest occupied valence band is completely occupied, therefore it is a continuous function. Smearing is one of the ways to make a discontinuous function in metal continuous by smearing out the edge using a smearing function, such as Fermi-Dirac function. The

range of smearing has to compromise between the computation efficiency and correctness: Too large will give wrong integration results on the total energy, while too small become useless therefore one needs more k-points.

### Basis set, cut-off energy

Now let us look back at equation (2.19), we can identify  $e^{i\mathbf{k}\cdot\mathbf{r}}$  as a plane wave,  $u_{\mathbf{k}}(\mathbf{r})$  is periodic in space and it can be expanded in terms of a set of plane waves as well:

$$u_{\mathbf{k}}(\mathbf{r}) = \sum_{\mathbf{G}} c_{\mathbf{G}} e^{i\mathbf{G}\cdot\mathbf{r}}, \quad (2.20)$$

where  $c_{\mathbf{G}}$  is the coefficient that determines the magnitude of the plane wave  $e^{i\mathbf{G}\cdot\mathbf{r}}$ . equation (2.19) can now exclusively be represented with plane waves:

$$\phi_{\mathbf{k}}(\mathbf{r}) = \sum_{\mathbf{G}} c_{\mathbf{k}+\mathbf{G}} e^{i\mathbf{k}+\mathbf{G}\cdot\mathbf{r}}. \quad (2.21)$$

The summation in the above equation, for practical reasons, has to be truncated. The truncation is usually done for the kinetic energy:

$$E = \frac{1}{2} |\mathbf{k} + \mathbf{G}|^2. \quad (2.22)$$

The maximum kinetic energy,  $E_{cut}$ , associates with a  $\mathbf{G}$  vector to limit the summations. Here we arrive at another convergence parameter: the plane wave cut-off energy. Similar to the  $\mathbf{k}$  points, it has to be large enough for the total energy to be converged in an acceptable precision range. While too large will cost more computational resources without additional benefits.

### Pseudopotentials and projected augmented-wave method

Considering the chemically inertness of the core electrons and their highly oscillating wave functions, their impact on the valence electrons is generally approximated by pseudopotentials in order to realize optimal computational efficiency. It is a smooth function and has the ability to reconstruct the original core electron properties. In practice, a pseudopotential is constructed for one isolated atom of one element. While being used in complex multi-elements system, the transferability of the pseudopotential is the key factor that determines how well

they will perform. Ultrasoft [106] and projected augmented-wave (PAW) [107, 108] are two types of the most popular pseudopotentials-based methods used in materials simulations. They are well-balanced between accuracy and computational cost. In this thesis, the PAW method is exclusive used for all calculations. This method combines the ideas of pseudopotentials method and all-electron methods. Same as in the case of pseudopotential, in PAW, the true wave function  $|\Psi_n\rangle$  that are obtained from all-electron methods can be transformed into a smooth auxiliary function  $|\tilde{\Psi}_n\rangle$  by a linear transformation operator  $\mathcal{T}$ . The partial waves  $|\phi_i\rangle$  is the complete basis set that expands the wave function can be also related to auxiliary partial waves  $|\tilde{\phi}_i\rangle$ :

$$|\phi_i\rangle = \mathcal{T} |\tilde{\phi}_i\rangle, \quad (2.23)$$

where  $i$  is a complete set of quantum numbers. The true and the auxiliary wave functions are identical outside the cur-off radius  $r_c$ :

$$\phi_i(\mathbf{r}) = \tilde{\phi}_i(\mathbf{r}), \text{ for } |\mathbf{r} - \mathbf{R}| > r_c, \quad (2.24)$$

where  $\mathbf{R}$  is the position of the atom. The transformation operator  $\mathcal{T}$  takes the following form:

$$\mathcal{T} = 1 + \sum_i (|\phi_i\rangle - |\tilde{\phi}_i\rangle) \langle \tilde{\rho}_i |, \quad (2.25)$$

where  $\tilde{\rho}_i$  is projector functions that capture the character of true wave function within a radius of  $r_c$ . Now the all-electron wave functions can be reconstructed through the smooth auxiliary functions and projector functions :

$$|\Psi_n\rangle = |\tilde{\Psi}_n\rangle + \sum_i (|\phi_i\rangle - |\tilde{\phi}_i\rangle) \langle \tilde{\rho}_i | \tilde{\Psi}_n \rangle. \quad (2.26)$$

The PAW method expresses the true all-electron wave functions with smooth functions that can be easily implemented and perform more efficiently as compared to the all-electron wave functions, moreover the accuracy of the calculations are comparable to the all-electron ones.

### 2.2.1 Software Packages

There are more than 70 different software packages capable of performing density functional theory calculations according to Wikipedia[109]. They mainly differ in type of pseudopotentials if there is any, what type of basis set is used to expand the wave function, in which programming language it is written and whether or not it is free or commercial etc. Lejaeghere et al. [110] have compared 40 different implementations and their accuracy by comparing their results to a highly accurate all-electron method. They concluded that all codes or methods yield generally consistent results. The accuracy of the codes which were developed in recent years is higher than the earlier ones. The Vienna *Ab initio* Simulation Package (VASP) [111, 112] with its projected augmented-wave method is one of the most accurate codes concluded from this study. Its well-optimized performance on supercomputers gives good results in less time as compared with the others. This code will be used as the main tool for all the calculations done in this thesis.



# **Chapter 3**

## **General physical properties 2D materials**

In this thesis, the properties of materials are divided into a preliminary and an advanced category, where the latter will be presented in the next chapter as the main results of this thesis. In this chapter, I will focus on the preliminary properties of 2D materials, namely structural, electronic, vibrational and mechanical properties. These properties are considered as test calculations and knowledge upon which the advanced properties are closely relied on. They are composed both of my original calculations and results from literature. An emphasis will be made on the characteristic properties of 2D materials that are different for 3D cases.

### **3.1 Structural properties**

#### **3.1.1 Layer structure**

As discussed in the chapter 1 Introduction, layered bulk materials have a close relationship with 2D materials. The strong anisotropic structure in the former results in the layer concept in the latter, and a single layer of a layered bulk material is a 2D material. This anisotropic nature is attributed to the weak interlayer bonds and the strong intralayer bonds. Van der Waals (vdWs) interactions [113] are the main types of these weak interlayer bonds. vdWs interactions are the attraction and the repulsion between atom or molecule entities caused by dipole-

dipole, dipole-induced dipole and instantaneous induced dipole-induced dipole forces. The definition is sometimes extended to include all dispersion forces between molecules. For 2D materials, vdWs interactions become important as the number of layers is larger than one; that is few-layer materials having typically less than ten layers. They also belong to the family of 2D materials since the thickness of the materials still small for quantum confinements to dominate their roles. As in its layered bulk counterpart, a few-layer system is a stack of monolayers that hold together through vdWs forces. When no other bonding types are present, interlayer vdWs interactions determine all the change brought by going above a single layer, and their impact on the electronic structure can be significant. For example, from monolayer to bilayer, the linear dispersion relation of energy  $E$  and momentum  $k$  around the  $K$  point evolves into parabolic-like spectrum[114, 115].

In Fig. 3.1 (a), the dispersion relation of graphite along the  $z$  direction, that is the HKH line in the Brillouin zone, is shown on the blue plane. This direction is perpendicular to the graphite layers. Because of the interlayer interaction and the quantum confinements, in few-layer system, the finite thickness limits the number of wave vectors that standing waves can take. Therefore, if only the intralayer and interlayer interactions between the nearest neighbour atoms were considered, the dispersion relations in few-layer systems can be approximated as those on the cross-section of red planes with the 3D graphite dispersion relation, see Fig. 3.1 (a). These planes are perpendicular to the  $z$  direction and intersect with the HKH line at limited points. This is called the zone-folding of dispersion relations[116]. These points are illustrated in Fig. 3.1 (c). Under the condition that quantum confinements at a few-layer system require that the wave functions vanish at the imaginary layer right outside the surface of the system, the systems will have well-defined wave vectors. Then, the dispersion relations of graphene and bilayer graphene will be on the red planes that intersect the HKH line at  $k_z = \pi/c$  and at  $k_z = 2(\pi/3c)$ , respectively. Having the knowledge of 3D band structure of graphite, we can approximate the dispersion relation of few-layer systems in this way. As a result, as shown in red plane in Fig. 3.1 (a) and their 3D version in Fig. 3.1 (b), graphene has linear dispersion relations and bilayer graphene has two parabolic-like bands that come from each layer. Moreover, the bilayer structure will never pass through the  $H$  point where graphene

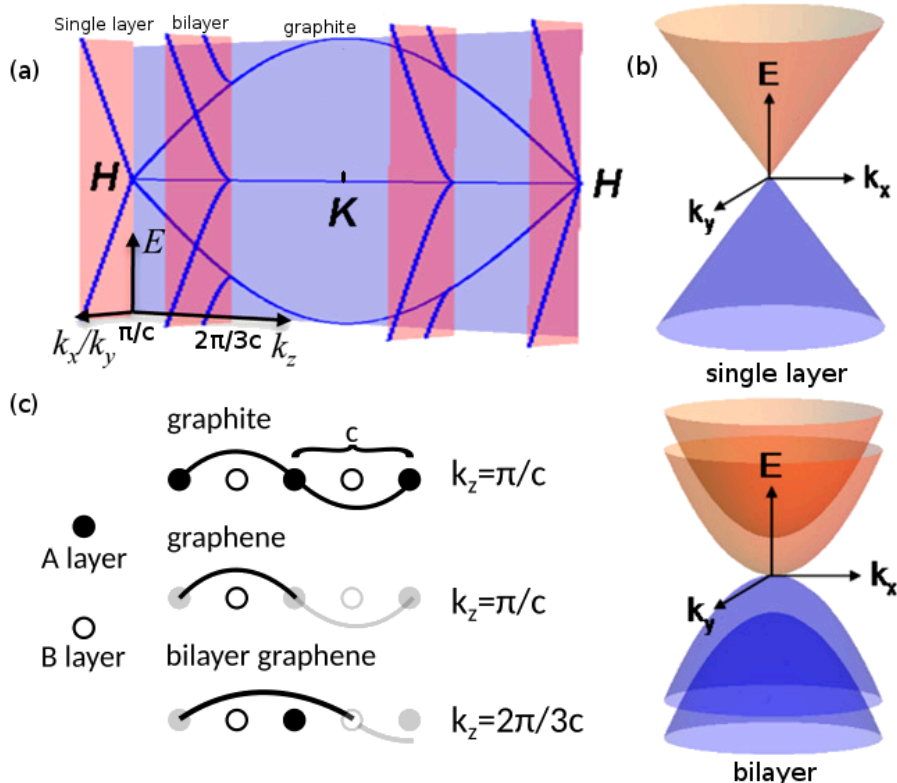


Fig. 3.1 (a) Energy-momentum dispersion relations of single layer and bilayer graphene as approximated by plane intersections of 3D graphite dispersion relation and (b) their 3D dispersion relations around the  $K$  k point. (c) Matching of the wavelength in graphite to that in single layer and bilayer graphene. Image adapted from: [115].

has passed to have linear dispersion relations. This is because that the standing waves in bilayer will have a wave vector  $k = 2(n\pi/3c)$ , where  $n$  is a positive integer: 1, 2, ...,  $n$ . This will never equal to  $\pi/c$  for any integer number of  $n$ . More generally, systems with an even number of layers will not have a linear dispersion relation, and vice versa for systems that have an odd number of layers. Further, if other interactions were considered, an overlap of those bands touching each other would have occurred[114]. This overlap increases with the number of layers. Eventually in graphite, maximum overlap is reached.

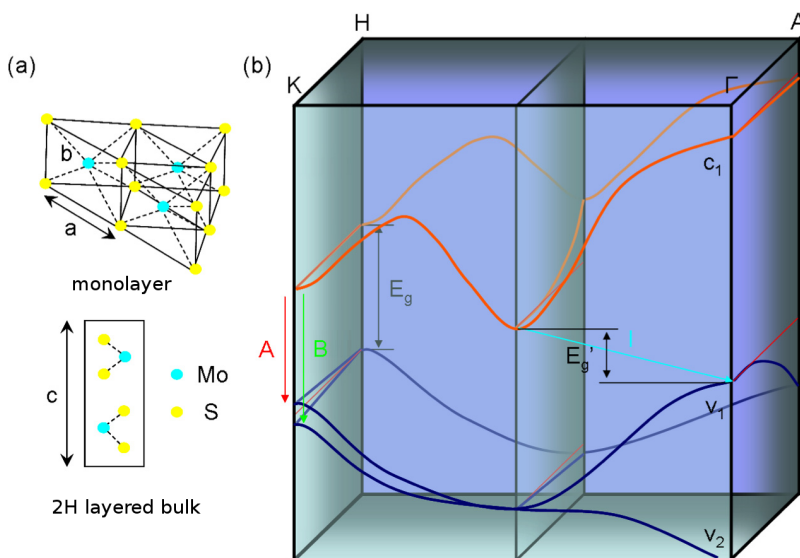


Fig. 3.2 Energy-momentum dispersion relations of MoS<sub>2</sub> as plane intersections of 3D dispersion relations. Image adapted from: [117].

Another example of the importance of interlayer interactions in few-layer 2D materials is for MoS<sub>2</sub>. As mentioned in the chapter 1 Introduction, as going from layered bulk to monolayer, MoS<sub>2</sub> transforms from an indirect band gap to a direct one. Here again, we can make use of the zone-folding scheme to approximate the band structure of the monolayer from that of the layered bulk. The monolayer and the layered bulk structure of 2H phase are shown in Fig. 3.2 (a). In figure (b), let us focus on the planes parallel to the page that pass through the KΓ line and the HA line (simply call them KΓ plane and HA plane below). Similar to the previously discussed graphite, 2H layered bulk MoS<sub>2</sub> has two layers per unit cell. Therefore, according to the standing wave arguments that we have used for the graphene case above, HA plane represents the monolayer.  $E_g$  and

$E_{I_g}$  are the band gaps of the monolayer and the layered bulk structures. Here, not only the magnitude of the band gap is increased as going from layered bulk to monolayer, the character of the band gap has changed as well. It is clearly shown that this is due to the band edges shifting. VBM at  $\Gamma$  and CBM at the middle of  $\Gamma K$  line are brought closer as they go from monolayer to layered bulk. This corresponds to the widening of band width and it is coming from the splitting of the VB and CB when more and more layers interact with each other through the interlayer interactions. Therefore, band gap in the layered bulk is defined by these two band edges, which in the monolayer was defined by band edges at  $K$ . In contrast to this, the band edges at the  $K$  are not affected too much by the interlayer interaction to make a difference. So why do the band edges react differently to the interlayer interactions? If we look into the orbital composition of the band edges, we will find that the ones that have widened the most, i.e. VBM at  $\Gamma$ , have the largest contribution from S  $p_z$  and Mo  $d_{z^2}$  orbitals. These out-of-plane orbitals vertically orientate to the plane and thus have maximum overlap with the others from an adjacent layer. Therefore, band splitting is more profound for these band edges and causing the widen of their band width. In contrast, both of the CBM and VBM at  $K$  are largely composed of S  $p_x$  and  $p_y$  orbitals and Mo  $d_{xy}$  and  $d_{x^2-y^2}$  orbitals. All of them are in-plane orientated orbitals and thus have limited effect from interlayer interactions[118].

### 3.1.2 sp hybridization

After discussing layered structure and the importance of interlayer interaction, let us look into some details of the in-plane structures and how sp hybridization gives rise to various structures for 2D materials. When atoms come together to form bonds, the orientations of bonding orbitals are decisive for the final structure. The sp hybridization is a good example of this. It mainly exists in three different variants: sp,  $sp^2$  and  $sp^3$ , see Fig. 3.3. The hybridization index  $n$  in  $sp^n$  stands for the relative amount of p character in the resulting hybridized orbital. For example,  $sp^2$  has 1/3 s character and 2/3 p character. Hybridized orbitals tend to maximize their distance to reduce the energy raised by the repulsion of electrons. As shown in Fig. 3.3, this results in tetrahedral structure of  $sp^3$  orbitals, as in diamond, trigonal planar structure of  $sp^2$  orbitals, as in graphene or

graphite and linear structure of sp orbitals, as in ethyne molecules. This is, for example, useful to explain the buckled structure of graphane and fluorographene. Because of  $sp^3$  character developed when the fourth electrons are bonded with H or F atoms, buckling appears in these systems.

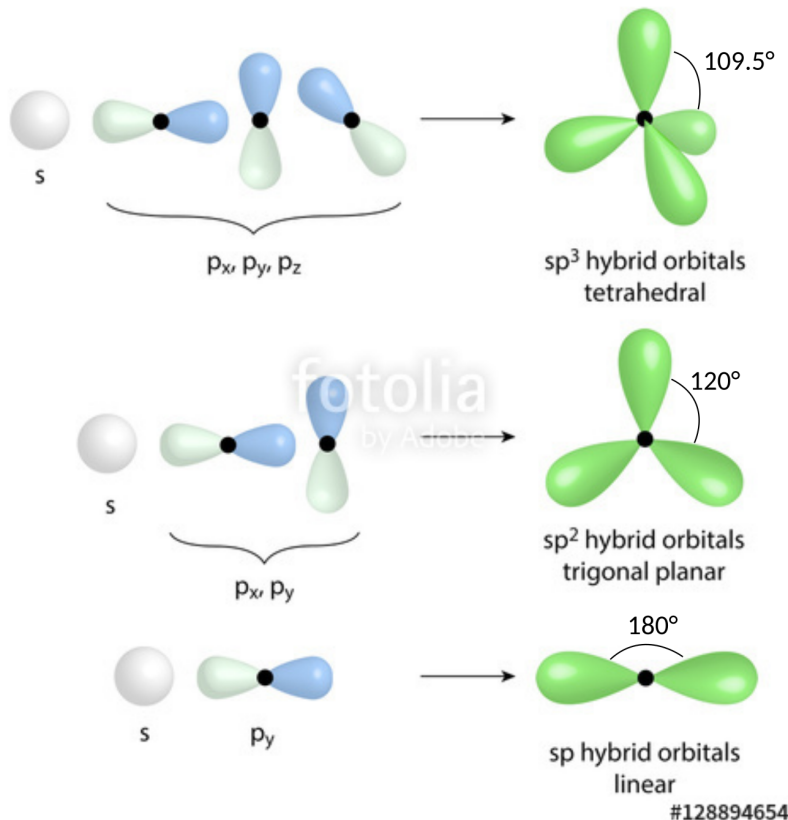


Fig. 3.3 Three types of sp hybridized orbitals. Image adapted from: [119].

Coulson and Moffitt [120] generalized the relation of bond angle with  $n$  as follows:

$$1 = -\sqrt{n_1 n_2} \cos\theta_{12}, \quad (3.1)$$

where  $\theta_{12}$  is the bond angle between orbital 1 and 2. The bond angle can be measured in the structures after the relaxation simulations. If orbital 1 and 2 have different  $n_1$  and  $n_2$ , we still need one more constraint to solve the equation (3.1) for the hybridization indices  $n$ . This constraint is that, in the case of carbon atom, the total portions of s orbital should equal to 1, while it should be 3 for the p orbitals. With these pieces of knowledge, the equation (3.1) can be

solved, and each orbital from one atom can be assigned with a  $n$ . This formula is useful to determine the s and p fractions of the bonds. For example,  $\theta_{12} = 90^\circ$  gives  $n \rightarrow \infty$ , which means it is a pure p orbital;  $\theta_{12} = 120^\circ$  gives  $n = 2$ , that is a  $sp^2$  hybridized orbital. Generally, the wider the bond angle, the larger the s contribution. Accordingly, bond angles are ordered as  $sp > sp^2 > sp^3$ . Of course, the equation (3.1) is more useful when the bond angle takes values other than those three types of hybridized orbitals mentioned, then it can be used to explain the resulting geometry.

## 3.2 Electronic properties

Electronic properties is one of the first features we would like to know about new materials. Not only is it because semiconductor and metal have different roles in the applications, but also because details of the electronic structure set the direction towards which further exploration should be carried out. One example for this from my experience is that by monitoring electronic structure variations under strain, we had predicted how the mobility of the carrier can be tuned. This will be discussed in the later chapters. Therefore, it is important to understand this property of a new material to fully reveal its potential. Electronic properties are usually characterized by band structure (BS) and density of states (DOS). These calculations are standard calculations in common first-principles codes from where all subsequent calculations start. After solving the Kohn-Sham equation with properly defined cut-off energy, k points etc., we will have the eigenenergy of each state that are indexed with k point in the Brillouin zone and band. DOS is a count of such states at specific energy. BS is the plot of eigenenergy along the lines in the Brillouin zone that connect high symmetry k points. 2D material has vast variation of electronic properties, from semimetallic graphene to semiconducting MoS<sub>2</sub> and to insulating BN. I will briefly discuss this at the end of this section. The purpose of this section is to point out some of the interesting electronic properties of some 2D materials. We will start with a brief introduction to the electronic properties of graphene.

### 3.2.1 Graphene

As mentioned before, orbitals of the C atoms in graphene are  $sp^2$  hybridized. Each one of these  $sp^2$  orbitals, coloured in green in Fig. 3.4, is composed from s,  $p_x$  and  $p_y$  orbitals, whereas the  $p_z$  orbital, coloured in yellow in the figure, is left unchanged. One  $sp^2$  hybridized orbital with another one from an adjacent atom form a strong  $\sigma$  bond, while  $p_z$  orbitals form  $\pi$  bonds. It may look like alternative single and double bonds between atoms, however, according to the Clar's theory, the bond order, i.e. the number of chemical bonds between a pair of atoms, in graphene is  $4/3$  and it is uniform[121]. This has to do with the high symmetry of graphene lattice.

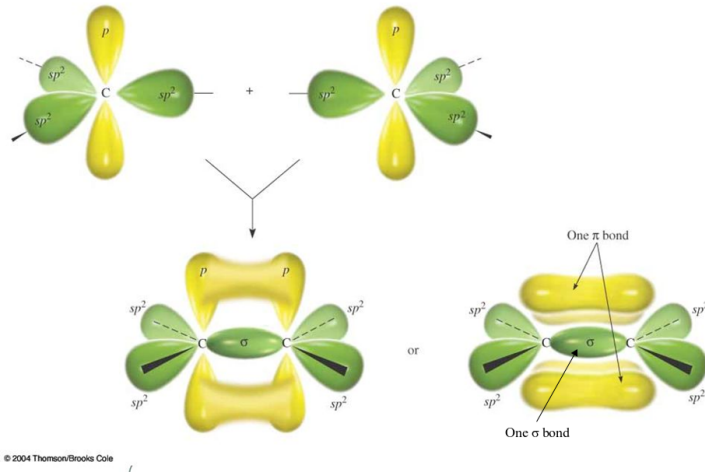


Fig. 3.4 The formation of  $sp^2$   $\sigma$  and  $p_z$   $\pi$  double bond. Image source: [122].

Every C atom has same local environment in graphene, however, adjacent atoms are not equivalent from the symmetry point of view. They belong to different hexagonal sublattices A and B as indicated with blue and yellow colors in Fig. 3.5.  $a_1$  and  $a_2$  are the basis vectors in real space connecting equivalent lattice sites. On the left,  $b_1$  and  $b_2$  are the basis vectors in reciprocal space connecting equivalent k points. The hexagon in the reciprocal space is the first Brillouin zone where all inequivalent k points are contained. These k points associate with different parallel lines of atoms and thus their directions in the reciprocal space are associated with different directions in real space. The k wave vectors near the

$\Gamma$  point have longer wave length than those away from it. While those at the boundary of the first Brillouin zone have wave lengths that are two times the unit cell dimension on the direction specified by the  $k$  points. For example, the most interesting  $k$  point for graphene is the  $K$  and  $K'$  points. These directions correspond to the  $a_1$  and  $a_2$  directions in real space. It is only at these  $k$  points in the Brioulloin zone that the antibinding and the bonding  $\pi$  band touch each other.

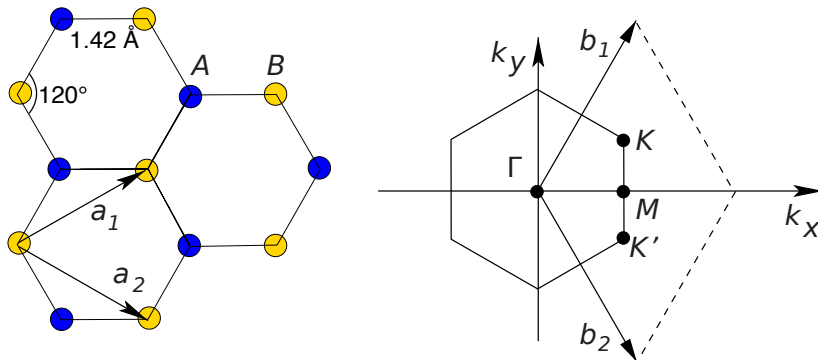


Fig. 3.5 Graphene lattice and its Brillion zone. Image source: [14].

As compared to  $\pi$  bond, the  $\sigma$  bond originates from a strong overlap of  $sp^2$  orbitals. The interaction is so strong that the splitting of bonding and antibonding orbitals is large. This makes the  $\sigma$  bonding orbitals deep in energy, or in other words, makes the  $\sigma$  bond strong and difficult to break. This feature contributes the most to the mechanical strength of graphene. On the other hand,  $p_z$  orbitals are less overlapped. This makes the  $\pi$  bond energy close to Fermi level, i.e. the highest occupied state. Therefore, they contribute the most to the electronic properties of graphene.

### 3.2.2 Dirac cone and symmetry

We have seen that graphene, silicene and germanene have an interesting electronic structure: Dirac cone. We also have listed the consequences of having such a feature: high mobility, massless carrier etc. In this section, we will discuss the symmetry condition for the existence of Dirac cones. This knowledge can be used to discover more materials with Dirac cone. According to von Neumann-Wigner theorem, the space-time inversion symmetry is crucial for the existence

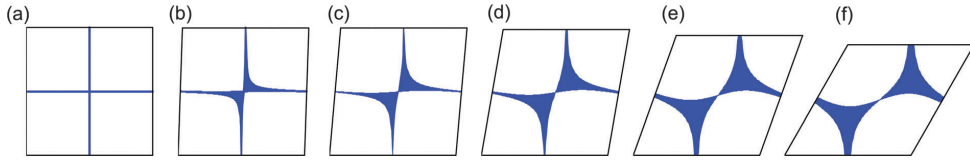


Fig. 3.6 Possible positions for the second atom (blue area) in order to guarantee the existence of Dirac cones as going from (a) square lattice to (f) hexagonal lattice. The first atom is located at the corners of the unit cell. Image source: [123].

and protection of Dirac cones[124]. It is a combination of space inversion and time reversal symmetries. These two are equally important and have to act simultaneously for the possible formation of Dirac cones. A more restrictive condition that guarantees the existence of Dirac cones has to deal with relations of hopping integrals[125, 123]. It is from the Liu, Wang, and Li [123]'s study that it revealed that the hexagonal lattice has the most favourable structure to form Dirac cones. The probability decreases as one goes from a hexagonal lattice to a square lattice, as shown in Fig. 3.6. Therefore, since most of the 2D materials have hexagonal symmetry, there will be a higher chance of finding materials with Dirac cones in this category.

### 3.2.3 Examples: 2D h-BN, 2D MoS<sub>2</sub> and graphene

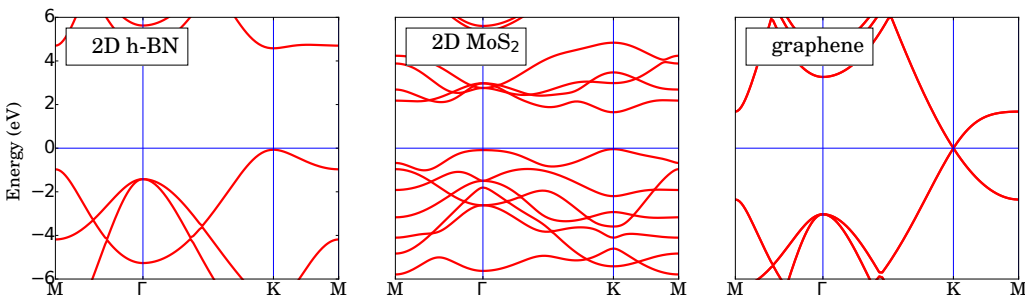


Fig. 3.7 Electronic band structures of 2D-hBN, 2D-MoS<sub>2</sub> and graphene calculated with PBE-GGA functional.

Three typical examples of the band structures of 2D materials are shown in Fig. 3.7. The 2D h-BN acts as an insulator due to a large band gap in the ultraviolet range, therefore it is suitable to serve as a dielectric layer in an electronic device.

The 2D TMDs have a band gap ranging from 1.0-2.5 eV which is in the visible and the near infrared range of light, therefore, it is suitable for optoelectronic device applications. Furthermore, we can see as we compare the dispersion curves along the  $M\Gamma$  and  $K\Gamma$ , the electronic structures are generally the same on these paths which correspond to different crystallographic directions. This means the materials in the figure are highly isotropic, thus we would expect the same for the physical properties. In the results chapters of this thesis, we will see some new 2D materials that are highly anisotropic. Their discoveries enrich the features of the physical properties of 2D materials.

### 3.3 Vibrational properties

Vibrational property is an important aspect of the materials, especially at finite temperature. Thermal expansion, thermal conductivity and electron mobility are all vibrational related topics. Therefore, it is crucial to understand the characterization of this in computational modelling. The force on an atom can be calculated from the wave functions evaluated from DFT thanks to the Hellmann-Feynman theorem. When searching for the equilibrium geometry of the materials, one basically is trying different positions of atoms to find a geometry that minimizes all the forces. This usually is the first thing to do for new materials, since different codes, implementations and, more importantly, different functionals will give different results. Despite the fact that the difference is usually small, unrelaxed geometry will have residual forces on the atoms. This is particularly important when vibrational properties are concerned. Vibrational properties are characterized through the energy (usually expressed in terms of frequency) versus vibrational wave vector dispersion relations. In crystal, all atoms have their equilibrium positions that coincide with the lattice points. Atoms vibrate around these positions. The vibrational modes are quantized into phonons. Each phonon represent a periodic, collective vibration with a well-defined vibrational mode and wave vector. The forces ( $F$ ) that restore the atoms when they deviate from their equilibrium positions can be calculated from DFT either by introducing small displacement or from perturbation theory. Then, the force constants,  $\Phi$ , can be constructed by monitoring the change in forces through the displacements,  $u$ , of atoms in the following way:

$$\Phi_{i\alpha,j\beta} = \frac{\partial F_{j\beta}}{\partial u_{i\alpha}}, \quad (3.2)$$

where the  $i, j$  indices are the labels for atoms,  $\alpha, \beta$  are the Cartesian directions:  $x, y$  and  $z$ . The Fourier transformation of the force constants at wave vector  $\mathbf{q}$  is the dynamical matrix  $D(\mathbf{q})$  that is related to the frequency of the phonon through the eigenvalue problem:

$$\omega^2(\mathbf{q}, n)\mathbf{e}(\mathbf{q}, n) = D(\mathbf{q})\mathbf{e}(\mathbf{q}, n), \quad (3.3)$$

where  $\omega(\mathbf{q}, n)$  is the frequency of the phonon in mode  $n$  having a wave vector  $\mathbf{q}$ , and  $\mathbf{e}(\mathbf{q}, n)$  is the eigenvector[126, 127]. Depending on whether atoms in the unit cell are vibrating in-phase or out-of-phase, phonon modes are categorized into acoustic and optical, respectively. For polar materials, polarized atoms that vibrate with respect to each other can interact with light, it is the reason that these types of vibrations are called optical modes. Further, considering the respective directions of the wave ( $\mathbf{e}$ ) and vibration ( $\mathbf{q}$ ), the modes are subcategorized into transverse optical (TO) modes and transvers acoustic (TA) modes, where  $\mathbf{q} \perp \mathbf{e}$ , and longitudinal optical (LO) and longitudinal acoustic (LA) modes, where  $\mathbf{q} \parallel \mathbf{e}$ . These modes are all in-plane vibrations for 2D materials. For 2D materials, another direction is different from those in-plane ones, namely the  $\mathbf{c}$  lattice vector direction perpendicular to the 2D plane. Special modes exist: out-of-plane transverse optical (ZO) and out-of-plane transverse acoustic (ZA) ( $\mathbf{q} \perp \mathbf{e}$  and  $\mathbf{q} \parallel \mathbf{c}$ ). The total number of acoustic modes is three, that of optical modes is  $3N-3$ , where  $N$  is the total number of atoms in the unit cell.

### 3.3.1 Example: monolayer MoS<sub>2</sub>

Let us now take an example of layered bulk and monolayer MoS<sub>2</sub> to highlight some of the important details of phonon dispersion relations. A comparison of vibrational modes between layered bulk and monolayer MoS<sub>2</sub> is presented in Fig. 3.8 (a). First of all, the number of atoms in the unit cell reduces from six to three from layered bulk to monolayer. Therefore, the number of the optical modes will be reduced as well from 15 in the layered bulk to six in the monolayer. In the Fig. 3.8 (a) it is shown, as the material is transformed to the monolayer,

several modes merge with others that only differ by whether the vibration in different layers is in-phase or out-of-phase. Secondly, a characteristic feature of phonon disperions for layered bulk and 2D materials has appeared, namely the quadratic ZA mode (flexural mode). It is usually linear in 3D bulk materials because of strong interlayer interactions. Because in layered bulk, the interlayer interactions are weak and absent in 2D materials, therefore, it will cost less energy for the out-of-plane vibration and the quadratic dispersion will appear. As shown in Fig. 3.8 (b), phonons with longer wave lengths, i.e. around  $\Gamma$ , in ZA mode have smaller frequencies or energies. This means this mode is more easily excited at low temperature and forms ripples which can be often observed in 2D materials. The formation of ripples is crucial for the stability of 2D materials at a finite temperature. Lastly, in the projected DOS, the projections of mode eigenvectors to in-plane (XY) and out-of-plane (Z) components are shown. The modes with Z components, i.e. ZO<sub>1</sub>, ZO<sub>2</sub> and ZA, contribute the most to the Z projections, and vice versa for the longitudinal and acoustic modes to XY projection.

### 3.3.2 Dynamic stability from phonon dispersion

One of the most important outputs of phonon dispersion is the check on the dynamical stability of the structure. An unstable structure is usually indicated by the imaginary frequencies of its phonon dispersion in a portion of or throughout its Brillouin zone, see Fig. 3.9 for example.

Now let us try to understand it and make use of it to convert the unstable to a stable structure. Consider a relaxed structure in which forces on all atoms have vanished. This could be on a convex or on a concave of the potential energy surface (PES), see Fig. 3.10. Note that, in both situations, the forces, the derivative of the PES curves, are zero. Therefore, both situations can occur when the structure is relaxed only following the forces. In the case of PES convex, the dynamical matrix  $D(\mathbf{q})$  will have negative components because the direction of the force is same as the displacement. We have seen from equation (3.3) that  $D(\mathbf{q})$  is related to the square of frequency  $\omega$ , hence imaginary frequencies are the only solutions. However, a structure with imaginary frequencies near  $\Gamma$  q point does not necessarily mean it is not stable. Since a large supercell consisted of multi-

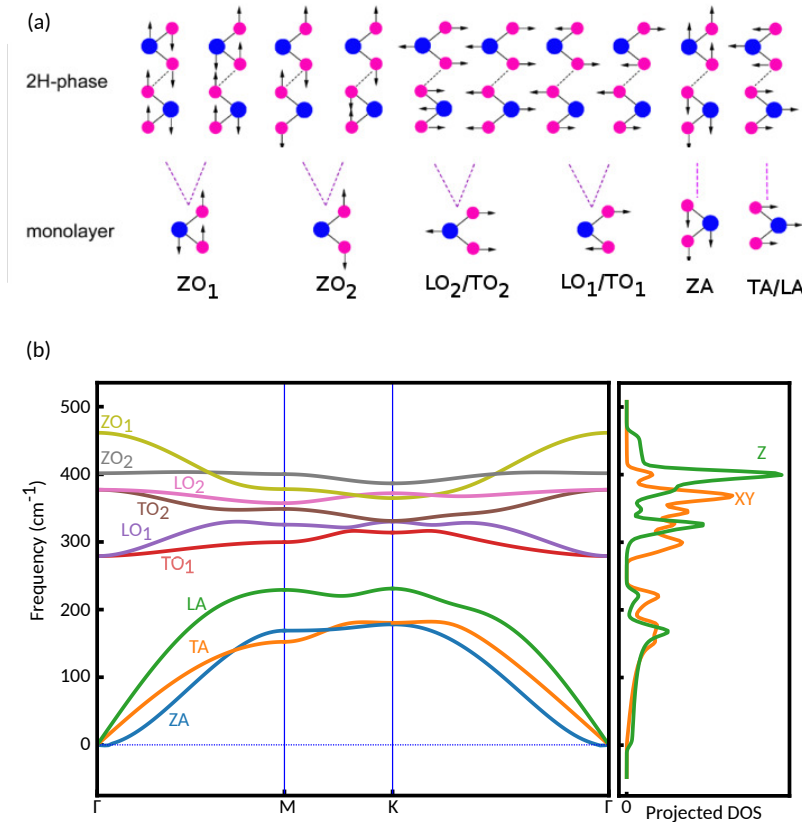


Fig. 3.8 (a) phonon modes of layered bulk (first row) and monolayer (second row) MoS<sub>2</sub> at  $\Gamma$  q point. (b) phonon dispersion and projected DOS of monolayer MoS<sub>2</sub>.

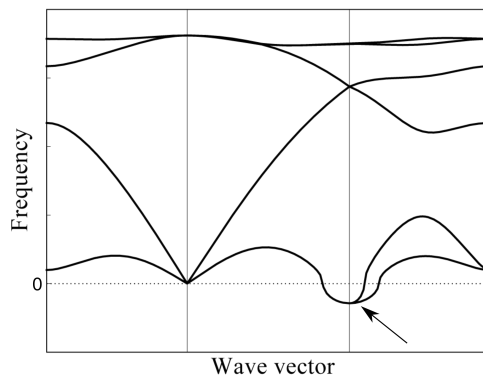


Fig. 3.9 Imaginary frequencies are shown as negative frequencies in a phonon dispersion plot.

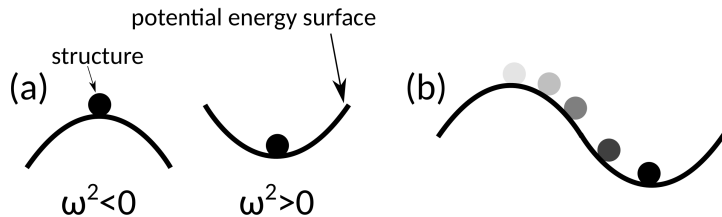


Fig. 3.10 (a) A structure at the convex (left) and the concave (right) of the PES. (b) Searching for a stable structure (phase transition).

ples of the unit cell is typically used to do phonon calculations, it may be that the size of the supercell is not large enough to correctly describe long wavelength phonons. Contrasted to this, a structure with imaginary frequencies that appear around other  $q$  points than  $\Gamma$  would imply a structure instability or a structural phase transition. The lowering of energy with some vibrational modes means the structure prefers the modulation induced by vibration, therefore if we calculate the energy of the modulated structure we will have a lower energy structure. With advanced techniques in phonon software[e.g. 128], it is possible to modulate such a structure based on the vibration mode which has an imaginary frequency to find a lower energy state and stabilize the structure, as schematically illustrated in Fig. 3.10 (b).

## 3.4 Mechanical properties

In chapter 1 Introduction, we have seen the stiffness and strength of some of the 2D materials. They all belong to the mechanical properties of the materials. The force on the atoms or the stress  $\sigma$  on the the unit cells under a finite strain  $\epsilon$  are the typical outputs from common first-principles codes. Within the elastic regime of stress-strain relation, they can be related through elastic constant  $C$ :  $\sigma = C\epsilon$ , this is Hook's law.  $C$  is a  $6 \times 6$  matrix whose matrix elements has a form  $C_{ij}$ . The elements measure the resistance of materials in  $i$  direction to a deformation in  $j$  direction, where  $i$  and  $j$  are the index of stress and strain tensors, respectively. Under the Voigt notations, the indices have the following correspondence: 1 → xx, 2 → yy, 3 → zz, 4 → yz, 5 → zx, 6 → xy. The elastic constants can be simplified if the crystal symmetry and dimension are taken into account. For example, for 2D hexagonal lattice symmetry, Hook's law reads:

$$\begin{pmatrix} \sigma_1 \\ \sigma_2 \\ \sigma_6 \end{pmatrix} = \begin{pmatrix} C_{11} & C_{12} & 0 \\ C_{12} & C_{11} & 0 \\ 0 & 0 & (C_{11} - C_{12})/2 \end{pmatrix} \begin{pmatrix} \epsilon_1 \\ \epsilon_2 \\ \epsilon_6 \end{pmatrix}. \quad (3.4)$$

In this way, all elastic constants can be extracted from stress-strain data from first-principles calculations. Generally, it is more convenient to have one quantity to describe each aspect of the mechanical properties of materials. This is where Young's modulus  $Y$ , shear modulus  $G$  and Poisson's ratio  $\nu$  become useful. Following the previous notations, they are defined as

$$Y_\alpha = \frac{1}{S_{\alpha\alpha}}, \quad \alpha = 1, 2, 3. \quad (3.5)$$

$$\nu_{\alpha\beta} = -Y_\beta S_{\alpha\beta}, \quad \alpha, \beta = 1, 2, 3 \quad (\alpha \neq \beta). \quad (3.6)$$

$$G_{\gamma\gamma} = \frac{1}{S_{\gamma\gamma}}, \quad \gamma = 4, 5, 6, \quad (3.7)$$

where  $\mathbf{S} = \mathbf{C}^{-1}$  is the compliance matrix [e.g. 129]. Young's modulus and shear modulus give the stiffness of the materials when it responds to stretching and shearing deformation in particular directions and they stand for the hardness of the materials. Their unit in 2D is  $J/m^2$  or  $N/m$ . To make them comparable with conventional 3D materials, 2D modulus usually are converted into 3D ones by dividing the former by the thickness of the sheet. Poisson's ratio gives the ratio of the transverse to the axial strain. It represents how easy it is to change the shape of the material with respect to changing the volume. Liquid and rubber have a Poisson's ratio close to 0.5, which is the theoretical upper limit of this quantity and making them the easiest materials to change shape over volume. In contrast, a cork has a Poisson's ratio close to zero, meaning zero lateral expansion when compressed in other directions. Breaking strength/strain is a measure of maximum load limit that materials can withstand, and it is used to characterize how strong a material is. This quantity is usually obtained by continuously deforming the materials until they break and recording the maximum stress/strain, it can be done both experimentally and through simulations.

### 3.4.1 Example: graphene, 2D-BN and 2D-MoS<sub>2</sub>

In table 3.1, the mechanical properties of several 2D materials are shown, as well as that of steel for comparison. As mentioned, graphene is the strongest material ever measured. This is owing to its strong  $\sigma$  and  $\pi$  bonding. With similar bonding in BN, it shows comparable results as graphene. MoS<sub>2</sub> has lower stiffness and strength than the previous two due to weaker bonding, nevertheless, it is still much stronger than steel. The Poisson's ratio has an inverse relation with Young's modulus. This means graphene acts more like a cork than like a rubber as compared to MoS<sub>2</sub>.

Table 3.1 Mechanical properties of graphene, BN and MoS<sub>2</sub>

material	Young's modulus TPa	Breaking strength GPa	Poisson's ratio
graphene[23]	1.0±0.1	130±10	0.149[130]
2D-BN [131]	0.71–0.97	120–165	0.210
2D-MoS <sub>2</sub> [132]	0.27± 0.10	23	0.29 [133]
A36 steel[134]	0.2	0.4–0.55	0.26

### 3.4.2 Mechanical stability: Born stability criteria

Mechanical stability is a criteria for unstressed crystal stability, which is additional to dynamical stability. It was first point out by Born [135] in the 1940's., for that, it is often called "Born stability criteria". Its core concept is that elastic energy should be positive for any non-zero strains. Elastic energy  $U$  is related to the elastic constants  $C_{ij}$  in the following way:

$$U = U_0 + \frac{1}{2} V_0 \sum_{i=1, j=1}^6 C_{ij} \epsilon_i \epsilon_j, \quad (3.8)$$

where  $U_0$  is the equilibrium energy and  $V_0$  is equilibrium volume. According to Born's paper[135], the necessary and sufficient stability conditions are: 1)  $|\mathbf{C}| > 0$ ; 2) all eigenvalues of  $\mathbf{C}$  are positive; 3) Sylvester's criterion: the determinations of the upper-left  $k$  by  $k$  sub-matrices are positive; (4) an arbitrary set of minors of  $\mathbf{C}$  are positive. Mouhat and Coudert [136] formulated closed form expressions of this criteria for different crystal systems. Taking into account the symmetry of

these systems, the number of criteria reduce, and become very useful to check the mechanical stability of new crystal system. For example, for 2D hexagonal crystal, the criteria become:

$$C_{11} > |C_{22}|, C_{66} > 0. \quad (3.9)$$

# References

- [1] K. S. Novoselov et al. "Electric Field Effect in Atomically Thin Carbon Films". In: *Science* 306.5696 (2004), pp. 666–669. DOI: 10.1126/science.1102896 (cit. on p. 1).
- [2] K. S. Novoselov et al. "Two-dimensional atomic crystals". In: *Proceedings of the National Academy of Sciences of the United States of America* 102.30 (2005), pp. 10451–10453. DOI: 10.1073/pnas.0502848102 (cit. on pp. 1, 16).
- [3] A. K. Geim and K. S. Novoselov. "The rise of graphene". In: *Nat. Mater.* 6.3 (Mar. 2007), pp. 183–191. DOI: 10.1038/nmat1849 (cit. on pp. 1, 5, 6).
- [4] The Royal Swedish Academy of Sciences. *The Nobel Prize in Physics 2010 - Information for the public*. 2010. URL: [https://www.nobelprize.org/nobel\\_prizes/physics/laureates/2010/popular- physicsprize2010.pdf](https://www.nobelprize.org/nobel_prizes/physics/laureates/2010/popular- physicsprize2010.pdf) (visited on 04/14/2017) (cit. on p. 4).
- [5] H. Petroski. *The Pencil: A History of Design and Circumstance*. Knopf, 1990 (cit. on p. 3).
- [6] A. Krishnan et al. "Graphitic cones and the nucleation of curved carbon surfaces". In: *Nature* 388.6641 (July 1997), pp. 451–454. DOI: 10.1038/41284 (cit. on pp. 3, 5).
- [7] Y. Ohashi et al. "Size Effect in the In-plane Electrical Resistivity of Very Thin Graphite Crystals". In: *TANSO* 1997.180 (1997), pp. 235–238. DOI: 10.7209/tanso.1997.235 (cit. on pp. 3, 5).
- [8] M. S. Dresselhaus and G. Dresselhaus. "Intercalation compounds of graphite". In: *Advances in Physics* 51.1 (2002), pp. 1–186. DOI: 10.1080/00018730110113644 (cit. on p. 3).
- [9] H. Shioyama. "Cleavage of graphite to graphene". In: *Journal of Materials Science Letters* 20.6 (2001), pp. 499–500. DOI: 10.1023/A:1010907928709 (cit. on p. 3).
- [10] R. Peierls. "Quelques propriétés typiques des corps solides". fre. In: *Annales de l'institut Henri Poincaré* 5.3 (1935), pp. 177–222 (cit. on p. 3).
- [11] Lev Davidovich Landau. "On the theory of phase transitions. I." In: *Phys. Z. Sowjet.* 11 (1937), p. 26 (cit. on p. 3).

- [12] N. D. Mermin. "Crystalline Order in Two Dimensions". In: *Phys. Rev.* 176 (1 Dec. 1968), pp. 250–254. DOI: 10.1103/PhysRev.176.250 (cit. on p. 3).
- [13] P. R. Wallace. "The Band Theory of Graphite". In: *Phys. Rev.* 71 (9 May 1947), pp. 622–634. DOI: 10.1103/PhysRev.71.622 (cit. on pp. 3, 6).
- [14] a. H. Castro Neto et al. "The electronic properties of graphene". In: *Rev. Mod. Phys.* 81.1 (Jan. 2009), pp. 109–162. DOI: 10.1103/RevModPhys.81.109 (cit. on pp. 5, 41).
- [15] H. W. Kroto et al. "C<sub>60</sub>: Buckminsterfullerene". In: *Nature* 318.6042 (Nov. 1985), pp. 162–163. DOI: 10.1038/318162a0 (cit. on p. 5).
- [16] W. Krätschmer et al. "Solid C<sub>60</sub>: a new form of carbon". In: *Nature* 347.6291 (Sept. 1990), pp. 354–358. DOI: 10.1038/347354a0 (cit. on p. 5).
- [17] Sumio Iijima and Toshinari Ichihashi. "Single-shell carbon nanotubes of 1-nm diameter". In: *Nature* 363.6430 (June 1993), pp. 603–605. DOI: 10.1038/363603a0 (cit. on p. 5).
- [18] Ray H. Baughman, Anvar A. Zakhidov, and Walt A. de Heer. "Carbon Nanotubes—the Route Toward Applications". In: *Science* 297.5582 (2002), pp. 787–792. DOI: 10.1126/science.1060928 (cit. on p. 5).
- [19] K. S. Novoselov et al. "Two-dimensional gas of massless Dirac fermions in graphene". In: *Nature* 438.7065 (Nov. 2005), pp. 197–200. DOI: 10.1038/nature04233 (cit. on p. 6).
- [20] M. I. Katsnelson, K. S. Novoselov, and A. K. Geim. "Chiral tunnelling and the Klein paradox in graphene". In: *Nat Phys* 2.9 (Sept. 2006), pp. 620–625. DOI: 10.1038/nphys384 (cit. on p. 6).
- [21] K. S. Novoselov et al. "Room-Temperature Quantum Hall Effect in Graphene". In: *Science* 315.5817 (2007), pp. 1379–1379. DOI: 10.1126/science.1137201 (cit. on p. 6).
- [22] J Güttinger et al. "Transport through graphene quantum dots". In: *Reports on Progress in Physics* 75.12 (2012), p. 126502 (cit. on p. 7).
- [23] Changgu Lee et al. "Measurement of the Elastic Properties and Intrinsic Strength of Monolayer Graphene". In: *Science* 321.5887 (2008), pp. 385–388. DOI: 10.1126/science.1157996 (cit. on pp. 6, 49).
- [24] K.I. Bolotin et al. "Ultrahigh electron mobility in suspended graphene". In: *Solid State Communications* 146.9-10 (2008), pp. 351–355. DOI: 10.1016/j.ssc.2008.02.024 (cit. on p. 7).
- [25] K. I. Bolotin et al. "Temperature-Dependent Transport in Suspended Graphene". In: *Phys. Rev. Lett.* 101 (9 Aug. 2008), p. 096802. DOI: 10.1103/PhysRevLett.101.096802 (cit. on p. 7).
- [26] Alexander A Balandin et al. "Superior thermal conductivity of single-layer graphene". In: *Nano letters* 8.3 (2008), pp. 902–907 (cit. on p. 7).

- [27] Lijie Ci et al. "Atomic layers of hybridized boron nitride and graphene domains". In: *Nature Materials* 9.5 (Feb. 2010), pp. 430–435. DOI: 10.1038/nmat2711 (cit. on p. 7).
- [28] S Yi Zhou et al. "Substrate-induced bandgap opening in epitaxial graphene". In: *Nature materials* 6.10 (2007), pp. 770–775 (cit. on p. 7).
- [29] Edward McCann. "Asymmetry gap in the electronic band structure of bilayer graphene". In: *Physical Review B* 74.16 (2006), p. 161403 (cit. on p. 7).
- [30] Eduardo V Castro et al. "Biased bilayer graphene: semiconductor with a gap tunable by the electric field effect". In: *Physical review letters* 99.21 (2007), p. 216802 (cit. on p. 7).
- [31] D. C. Elias et al. "Control of Graphene's Properties by Reversible Hydrogenation: Evidence for Graphane". In: *Science* 323.5914 (2009), pp. 610–613. DOI: 10.1126/science.1167130 (cit. on pp. 7, 8).
- [32] Ki-Joon Jeon et al. "Fluorographene: A Wide Bandgap Semiconductor with Ultraviolet Luminescence". In: *ACS Nano* 5.2 (2011). PMID: 21204572, pp. 1042–1046. DOI: 10.1021/nn1025274 (cit. on pp. 7, 9).
- [33] SY Zhou et al. "Metal to insulator transition in epitaxial graphene induced by molecular doping". In: *Physical review letters* 101.8 (2008), p. 086402 (cit. on p. 7).
- [34] Kyoko Nakada et al. "Edge state in graphene ribbons: Nanometer size effect and edge shape dependence". In: *Phys. Rev. B* 54 (24 Dec. 1996), pp. 17954–17961. DOI: 10.1103/PhysRevB.54.17954 (cit. on p. 7).
- [35] Verónica Barone, Oded Hod, and Gustavo E. Scuseria. "Electronic Structure and Stability of Semiconducting Graphene Nanoribbons". In: *Nano Letters* 6.12 (2006). PMID: 17163699, pp. 2748–2754. DOI: 10.1021/nl0617033 (cit. on p. 7).
- [36] Zhiqiang Yang et al. "Birch Reduction of Graphite. Edge and Interior Functionalization by Hydrogen". In: *Journal of the American Chemical Society* 134.45 (2012). PMID: 23072630, pp. 18689–18694. DOI: 10.1021/ja3073116 (cit. on p. 8).
- [37] James S. Burgess et al. "Tuning the electronic properties of graphene by hydrogenation in a plasma enhanced chemical vapor deposition reactor". In: *Carbon* 49.13 (2011), pp. 4420–4426. DOI: 10.1016/j.carbon.2011.06.034 (cit. on p. 8).
- [38] Yu Wang et al. "Toward high throughput interconvertible graphane-to-graphene growth and patterning". In: *ACS nano* 4.10 (2010), pp. 6146–6152 (cit. on p. 8).
- [39] Duminda K. Samarakoon and Xiao-Qian Wang. "Chair and Twist-Boat Membranes in Hydrogenated Graphene". In: *ACS Nano* 3.12 (2009). PMID: 19947580, pp. 4017–4022. DOI: 10.1021/nn901317d (cit. on p. 8).

- [40] A.M. Ilyin et al. "Computer simulation and experimental study of graphane-like structures formed by electrolytic hydrogenation". In: *Physica E: Low-dimensional Systems and Nanostructures* 43.6 (2011), pp. 1262–1265. DOI: 10.1016/j.physe.2011.02.012 (cit. on p. 8).
- [41] Enrique Muñoz et al. "The ultimate diamond slab: GraphAne versus graphEne". In: *Diamond and Related Materials* 19.5-6 (2010). Proceedings of Diamond 2009, The 20th European Conference on Diamond, Diamond-Like Materials, Carbon Nanotubes and Nitrides, Part 1, pp. 368–373. DOI: 10.1016/j.diamond.2010.01.007 (cit. on p. 8).
- [42] J. Zhou et al. "Ferromagnetism in Semihydrogenated Graphene Sheet". Undetermined. In: *Nano Letters* 9.11 (Nov. 2009), pp. 3867–3870. DOI: 10.1021/nl9020733 (cit. on p. 8).
- [43] A. I. Shkrebtii et al. "Graphene and graphane functionalization with hydrogen: electronic and optical signatures". In: *physica status solidi (c)* 9.6 (2012), pp. 1378–1383. DOI: 10.1002/pssc.201100705 (cit. on p. 8).
- [44] Jorge O. Sofo, Ajay S. Chaudhari, and Greg D. Barber. "Graphane: A two-dimensional hydrocarbon". In: *Phys. Rev. B* 75 (15 Apr. 2007), p. 153401. DOI: 10.1103/PhysRevB.75.153401 (cit. on p. 9).
- [45] O Leenaerts et al. "First-principles investigation of graphene fluoride and graphane". In: *Physical Review B* 82.19 (2010), p. 195436 (cit. on p. 9).
- [46] Mingshan Zhu et al. "Fluorographene nanosheets with broad solvent dispersibility and their applications as a modified layer in organic field-effect transistors". In: *Phys. Chem. Chem. Phys.* 15 (48 2013), pp. 20992–21000. DOI: 10.1039/C3CP53383B (cit. on pp. 8, 9).
- [47] Duminda K. Samarakoon et al. "Structural and Electronic Properties of Fluorographene". In: *Small* 7.7 (Apr. 2011), pp. 965–969. DOI: 10.1002/smll.201002058 (cit. on p. 8).
- [48] Rahul R Nair et al. "Fluorographene: A Two-Dimensional Counterpart of Teflon". In: *small* 6.24 (2010), pp. 2877–2884 (cit. on p. 9).
- [49] Chun-Liang Lin et al. "Substrate-Induced Symmetry Breaking in Silicene". In: *Phys. Rev. Lett.* 110 (7 Feb. 2013), p. 076801. DOI: 10.1103/PhysRevLett.110.076801 (cit. on p. 10).
- [50] Lars Matthes, Olivia Pulci, and Friedhelm Bechstedt. "Massive Dirac quasi-particles in the optical absorbance of graphene, silicene, germanene, and tinene". In: *Journal of Physics: Condensed Matter* 25.39 (2013), p. 395305 (cit. on pp. 10, 11).
- [51] Sivacarendran Balendhran et al. "Elemental Analogues of Graphene: Silicene, Germanene, Stanene, and Phosphorene". In: *Small* 11.6 (2015), pp. 640–652. DOI: 10.1002/smll.201402041 (cit. on p. 10).
- [52] Joelson C. Garcia et al. "Group IV Graphene- and Graphane-Like Nanosheets". In: *The Journal of Physical Chemistry C* 115.27 (2011), pp. 13242–13246. DOI: 10.1021/jp203657w (cit. on p. 10).

- [53] Aaditya Manjanath, Vijay Kumar, and Abhishek K. Singh. "Mechanical and electronic properties of pristine and Ni-doped Si, Ge, and Sn sheets". In: *Phys. Chem. Chem. Phys.* 16 (4 2014), pp. 1667–1671. DOI: 10.1039/C3CP54655A (cit. on p. 11).
- [54] Patrick Vogt et al. "Silicene: compelling experimental evidence for graphene-like two-dimensional silicon". In: *Physical review letters* 108.15 (2012), p. 155501 (cit. on p. 11).
- [55] Linfei Li et al. "Buckled germanene formation on Pt (111)". In: *Advanced Materials* 26.28 (2014), pp. 4820–4824 (cit. on p. 11).
- [56] Chun-Liang Lin et al. "Structure of silicene grown on Ag (111)". In: *Applied Physics Express* 5.4 (2012), p. 045802 (cit. on p. 11).
- [57] Thaneshwor P Kaloni and Udo Schwingenschlögl. "Weak interaction between germanene and GaAs (0001) by H intercalation: a route to exfoliation". In: *Journal of Applied Physics* 114.18 (2013), p. 184307 (cit. on p. 11).
- [58] Nasim Alem et al. "Atomically thin hexagonal boron nitride probed by ultrahigh-resolution transmission electron microscopy". In: *Physical Review B* 80.15 (2009), p. 155425 (cit. on p. 11).
- [59] Houlong L Zhuang and Richard G Hennig. "Electronic structures of single-layer boron pnictides". In: *Applied Physics Letters* 101.15 (2012), p. 153109 (cit. on p. 12).
- [60] Alexey Bosak et al. "Elasticity of hexagonal boron nitride: Inelastic x-ray scattering measurements". In: *Phys. Rev. B* 73 (4 Jan. 2006), p. 041402. DOI: 10.1103/PhysRevB.73.041402 (cit. on p. 12).
- [61] Insun Jo et al. "Thermal Conductivity and Phonon Transport in Suspended Few-Layer Hexagonal Boron Nitride". In: *Nano Letters* 13.2 (2013). PMID: 23346863, pp. 550–554. DOI: 10.1021/nl304060g (cit. on p. 12).
- [62] Lu Hua Li and Ying Chen. "Atomically Thin Boron Nitride: Unique Properties and Applications". In: *Advanced Functional Materials* 26.16 (Apr. 2016), pp. 2594–2608. DOI: 10.1002/adfm.201504606 (cit. on p. 12).
- [63] Gwan-Hyoung Lee et al. "Flexible and Transparent MoS<sub>2</sub> Field-Effect Transistors on Hexagonal Boron Nitride-Graphene Heterostructures". In: *ACS Nano* 7.9 (2013). PMID: 23924287, pp. 7931–7936. DOI: 10.1021/nn402954e (cit. on p. 12).
- [64] DeanC R. et al. "Boron nitride substrates for high-quality graphene electronics". In: *Nat Nano* 5.10 (Oct. 2010), pp. 722–726. DOI: 10.1038/nnano.2010.172 (cit. on p. 12).
- [65] via Wikimedia Commons Benjah-bmm27 (Own work) [Public domain]. *Boron-nitride-(hexagonal)-side-3D-balls*. 2007. URL: [https://commons.wikimedia.org/wiki/File%3ABoron-nitride-\(hexagonal\)-side-3D-balls.png](https://commons.wikimedia.org/wiki/File%3ABoron-nitride-(hexagonal)-side-3D-balls.png) (visited on 05/02/2017) (cit. on p. 12).

- [66] Qing Hua Wang et al. "Electronics and optoelectronics of two-dimensional transition metal dichalcogenides". In: *Nat. Nanotechnol.* 7.11 (Nov. 2012), pp. 699–712. DOI: 10.1038/nnano.2012.193 (cit. on p. 13).
- [67] Z. Y. Zhu, Y. C. Cheng, and U. Schwingenschlögl. "Giant spin-orbit-induced spin splitting in two-dimensional transition-metal dichalcogenide semiconductors". In: *Phys. Rev. B* 84 (15 Oct. 2011), p. 153402. DOI: 10.1103/PhysRevB.84.153402 (cit. on p. 13).
- [68] Jaemyung Kim et al. "Enhanced Electrocatalytic Properties of Transition-Metal Dichalcogenides Sheets by Spontaneous Gold Nanoparticle Decoration". In: *The Journal of Physical Chemistry Letters* 4.8 (2013). PMID: 26282134, pp. 1227–1232. DOI: 10.1021/jz400507t (cit. on p. 13).
- [69] Yunpeng Huang et al. "Synthesis of few-layered MoS<sub>2</sub> nanosheet-coated electrospun SnO<sub>2</sub> nanotube heterostructures for enhanced hydrogen evolution reaction". In: *Nanoscale* 6 (18 2014), pp. 10673–10679. DOI: 10.1039/C4NR02014F (cit. on p. 13).
- [70] RadisavljevicB. et al. "Single-layer MoS<sub>2</sub> transistors". In: *Nat Nano* 6.3 (Mar. 2011), pp. 147–150. DOI: 10.1038/nnano.2010.279 (cit. on p. 13).
- [71] Gengzhi Sun et al. "Fabrication of Ultralong Hybrid Microfibers from Nanosheets of Reduced Graphene Oxide and Transition-Metal Dichalcogenides and their Application as Supercapacitors". In: *Angewandte Chemie* 126.46 (2014), pp. 12784–12788. DOI: 10.1002/ange.201405325 (cit. on p. 13).
- [72] Kun Chang and Weixiang Chen. "I-Cysteine-Assisted Synthesis of Layered MoS<sub>2</sub>/Graphene Composites with Excellent Electrochemical Performances for Lithium Ion Batteries". In: *ACS Nano* 5.6 (2011). PMID: 21574610, pp. 4720–4728. DOI: 10.1021/nn200659w (cit. on p. 13).
- [73] Dongyun Chen et al. "In situ nitrogenated graphene-few-layer WS<sub>2</sub> composites for fast and reversible Li<sup>+</sup> storage". In: *Nanoscale* 5 (17 2013), pp. 7890–7896. DOI: 10.1039/C3NR02920D (cit. on p. 13).
- [74] Yunguo Li et al. "Single-layer MoS<sub>2</sub> as an efficient photocatalyst". In: *Catal. Sci. Technol.* 3 (9 2013), pp. 2214–2220. DOI: 10.1039/C3CY00207A (cit. on p. 13).
- [75] Eric Parzinger et al. "Photocatalytic Stability of Single- and Few-Layer MoS<sub>2</sub>". In: *ACS Nano* 9.11 (2015). PMID: 26536283, pp. 11302–11309. DOI: 10.1021/acsnano.5b04979 (cit. on p. 13).
- [76] Liang Cheng et al. "PEGylated WS<sub>2</sub> Nanosheets as a Multifunctional Theranostic Agent for in vivo Dual-Modal CT/Photoacoustic Imaging Guided Photothermal Therapy". In: *Advanced Materials* 26.12 (2014), pp. 1886–1893. DOI: 10.1002/adma.201304497 (cit. on p. 13).
- [77] Wenyan Yin et al. "High-Throughput Synthesis of Single-Layer MoS<sub>2</sub> Nanosheets as a Near-Infrared Photothermal-Triggered Drug Delivery for Effective Cancer Therapy". In: *ACS Nano* 8.7 (2014). PMID: 24905027, pp. 6922–6933. DOI: 10.1021/nn501647j (cit. on p. 13).

- [78] Manish Chhowalla et al. "The chemistry of two-dimensional layered transition metal dichalcogenide nanosheets". In: *Nat. Chem.* 5.4 (Mar. 2013), pp. 263–275. DOI: 10.1038/nchem.1589 (cit. on p. 14).
- [79] Xinran Wang et al. "Room-Temperature All-Semiconducting Sub-10-nm Graphene Nanoribbon Field-Effect Transistors". In: *Phys. Rev. Lett.* 100 (20 May 2008), p. 206803. DOI: 10.1103/PhysRevLett.100.206803 (cit. on p. 14).
- [80] Melinda Y. Han et al. "Energy Band-Gap Engineering of Graphene Nanoribbons". In: *Phys. Rev. Lett.* 98 (20 May 2007), p. 206805. DOI: 10.1103/PhysRevLett.98.206805 (cit. on p. 14).
- [81] Young-Woo Son, Marvin L. Cohen, and Steven G. Louie. "Half-metallic graphene nanoribbons". In: *Nature* 444.7117 (), pp. 347–349. DOI: 10.1038/nature05180 (cit. on p. 15).
- [82] Prabhakar R. Bandaru. "Electrical Properties and Applications of Carbon Nanotube Structures". In: *Journal of Nanoscience and Nanotechnology* 7.4-1 (Apr. 2007), pp. 1239–1267. DOI: 10.1166/jnn.2007.307 (cit. on p. 15).
- [83] Jan Prasek et al. "Methods for carbon nanotubes synthesis-review". In: *J. Mater. Chem.* 21 (40 2011), pp. 15872–15884. DOI: 10.1039/C1JM12254A (cit. on p. 15).
- [84] Andrea C Ferrari et al. "Science and technology roadmap for graphene, related two-dimensional crystals, and hybrid systems". In: *Nanoscale* 7.11 (2015), pp. 4598–4810. DOI: 10.1039/C4NR01600A (cit. on p. 16).
- [85] Z. H. Ni et al. "On Resonant Scatterers As a Factor Limiting Carrier Mobility in Graphene". In: *Nano Letters* 10.10 (2010). PMID: 20795655, pp. 3868–3872. DOI: 10.1021/nl101399r (cit. on p. 17).
- [86] Neeraj Mishra et al. "Graphene growth on silicon carbide: A review". In: *physica status solidi (a)* 213.9 (2016), pp. 2277–2289. DOI: 10.1002/pssa.201600091 (cit. on p. 17).
- [87] Neeraj Mishra et al. "Graphene growth on silicon carbide: A review". In: *physica status solidi (a)* 213.9 (Sept. 2016), pp. 2277–2289. DOI: 10.1002/pssa.201600091 (cit. on p. 17).
- [88] Nicholas Petrone et al. "Chemical Vapor Deposition-Derived Graphene with Electrical Performance of Exfoliated Graphene". In: *Nano Letters* 12.6 (2012). PMID: 22582828, pp. 2751–2756. DOI: 10.1021/nl204481s (cit. on p. 18).
- [89] Sukang Bae et al. "Roll-to-roll production of 30-inch graphene films for transparent electrodes". In: *Nat Nano* 5.8 (Aug. 2010), pp. 574–578. DOI: 10.1038/nnano.2010.132 (cit. on p. 18).
- [90] Scott Kirklin et al. "The Open Quantum Materials Database (OQMD): assessing the accuracy of DFT formation energies". In: *npj Comput. Mater.* 1.1 (Dec. 2015), p. 15010. DOI: 10.1038/npjcompumats.2015.10 (cit. on p. 19).

- [91] P. Hohenberg and W. Kohn. "Inhomogeneous Electron Gas". In: *Phys. Rev.* 136 (3B Nov. 1964), B864–B871. DOI: 10.1103/PhysRev.136.B864 (cit. on p. 19).
- [92] W. Kohn and L. J. Sham. "Self-Consistent Equations Including Exchange and Correlation Effects". In: *Phys. Rev.* 140 (4A Nov. 1965), A1133–A1138. DOI: 10.1103/PhysRev.140.A1133 (cit. on p. 19).
- [93] Neil Drummond. *QMC Studies of Real Systems*. 2017. URL: <http://slideplayer.com/slide/4763755/> (visited on 05/10/2017) (cit. on p. 20).
- [94] M. Born and R. Oppenheimer. "Zur Quantentheorie der Moleküle". In: *Annalen der Physik* 389.20 (1927), pp. 457–484. DOI: 10.1002/andp.19273892002 (cit. on p. 21).
- [95] Mel Levy. "Universal variational functionals of electron densities, first-order density matrices, and natural spin-orbitals and solution of the v-representability problem". In: *Proceedings of the National Academy of Sciences* 76.12 (1979), pp. 6062–6065. DOI: 10.1073/pnas.76.12.6062 (cit. on p. 21).
- [96] John P Perdew. *Electronic structure of solids' 91*. Vol. 11. Akademie Verlag, Berlin, 1991 (cit. on p. 24).
- [97] John P. Perdew et al. "Atoms, molecules, solids, and surfaces: Applications of the generalized gradient approximation for exchange and correlation". In: *Phys. Rev. B* 46 (11 Sept. 1992), pp. 6671–6687. DOI: 10.1103/PhysRevB.46.6671 (cit. on p. 24).
- [98] John P. Perdew, Kieron Burke, and Matthias Ernzerhof. "Generalized Gradient Approximation Made Simple". In: *Phys. Rev. Lett.* 77 (18 Oct. 1996), pp. 3865–3868. DOI: 10.1103/PhysRevLett.77.3865 (cit. on p. 24).
- [99] Qian Peng, Fernanda Duarte, and Robert S. Paton. "Computing organic stereoselectivity - from concepts to quantitative calculations and predictions". In: *Chem. Soc. Rev.* 45 (22 2016), pp. 6093–6107. DOI: 10.1039/C6CS00573J (cit. on p. 25).
- [100] Carlo Adamo and Vincenzo Barone. "Toward reliable density functional methods without adjustable parameters: The PBE0 model". In: *The Journal of Chemical Physics* 110.13 (1999), pp. 6158–6170. DOI: 10.1063/1.478522 (cit. on p. 24).
- [101] Jochen Heyd, Gustavo E. Scuseria, and Matthias Ernzerhof. "Hybrid functionals based on a screened Coulomb potential". In: *The Journal of Chemical Physics* 118.18 (2003), pp. 8207–8215. DOI: 10.1063/1.1564060 (cit. on p. 24).
- [102] M J Lucero, T M Henderson, and G E Scuseria. "Improved semiconductor lattice parameters and band gaps from a middle-range screened hybrid exchange functional". In: *Journal of Physics: Condensed Matter* 24.14 (2012), p. 145504. DOI: 10.1088/0953-8984/24/14/145504 (cit. on p. 26).

- [103] David C. Langreth and John P. Perdew. “Theory of nonuniform electronic systems. I. Analysis of the gradient approximation and a generalization that works”. In: *Phys. Rev. B* 21 (12 June 1980), pp. 5469–5493. DOI: 10.1103/PhysRevB.21.5469 (cit. on p. 26).
- [104] C. Fiolhais, F. Nogueira, and M.A.L. Marques. *A Primer in Density Functional Theory*. Lecture Notes in Physics. Springer-Verlag Berlin Heidelberg, 2003. DOI: 10.1007/3-540-37072-2 (cit. on p. 27).
- [105] R. W. Godby, M. Schlüter, and L. J. Sham. “Self-energy operators and exchange-correlation potentials in semiconductors”. In: *Phys. Rev. B* 37 (17 June 1988), pp. 10159–10175. DOI: 10.1103/PhysRevB.37.10159 (cit. on p. 27).
- [106] David Vanderbilt. “Soft self-consistent pseudopotentials in a generalized eigenvalue formalism”. In: *Phys. Rev. B* 41 (11 Apr. 1990), pp. 7892–7895. DOI: 10.1103/PhysRevB.41.7892 (cit. on p. 30).
- [107] P. E. Blöchl. “Projector augmented-wave method”. In: *Phys. Rev. B* 50 (24 Dec. 1994), pp. 17953–17979. DOI: 10.1103/PhysRevB.50.17953 (cit. on p. 30).
- [108] G. Kresse and D. Joubert. “From ultrasoft pseudopotentials to the projector augmented-wave method”. In: *Phys. Rev. B* 59 (3 Jan. 1999), pp. 1758–1775. DOI: 10.1103/PhysRevB.59.1758 (cit. on p. 30).
- [109] *List of quantum chemistry and solid-state physics software*. 2017. URL: [https://en.wikipedia.org/wiki/List\\_of\\_quantum\\_chemistry\\_and\\_solid-state\\_physics\\_software](https://en.wikipedia.org/wiki/List_of_quantum_chemistry_and_solid-state_physics_software) (visited on 05/15/2017) (cit. on p. 31).
- [110] Kurt Lejaeghere et al. “Reproducibility in density functional theory calculations of solids”. In: *Science* 351.6280 (2016). DOI: 10.1126/science.aad3000 (cit. on p. 31).
- [111] G. Kresse and J. Hafner. “*Ab initio* molecular-dynamics simulation of the liquid-metal-amorphous-semiconductor transition in germanium”. In: *Phys. Rev. B* 49 (20 May 1994), pp. 14251–14269. DOI: 10.1103/PhysRevB.49.14251 (cit. on p. 31).
- [112] G. Kresse and J. Furthmüller. “Efficiency of *ab-initio* total energy calculations for metals and semiconductors using a plane-wave basis set”. In: *Computational Materials Science* 6.1 (1996), pp. 15–50. DOI: 10.1016/0927-0256(96)00008-0 (cit. on p. 31).
- [113] Johannes Diderik van der Waals. “Over de Continuiteit van den Gas- en Vloeistofoestand (on the continuity of the gas and liquid state)”. Ph.D. thesis. University of Leiden, 1873 (cit. on p. 33).
- [114] B. Partoens and F. M. Peeters. “From graphene to graphite: Electronic structure around the *K* point”. In: *Phys. Rev. B* 74 (7 Aug. 2006), p. 075404. DOI: 10.1103/PhysRevB.74.075404 (cit. on pp. 34, 36).

- [115] Kin Fai Mak et al. "The evolution of electronic structure in few-layer graphene revealed by optical spectroscopy". In: *Proceedings of the National Academy of Sciences* 107.34 (2010), pp. 14999–15004. DOI: 10.1073/pnas.1004595107 (cit. on pp. 34, 35).
- [116] R. Saito, G. Dresselhaus, and M.S. Dresselhaus. *Physical Properties of Carbon Nanotubes*. Imperial College Press, 1998 (cit. on p. 34).
- [117] K. F. Mak et al. "Atomically Thin MoS<sub>2</sub>: A New Direct-Gap Semiconductor". In: *Physical Review Letters* 105.13, 136805 (Sept. 2010). [The version from arXiv.org], p. 136805. DOI: 10.1103/PhysRevLett.105.136805 (cit. on p. 36).
- [118] J. E. Padilha et al. "Nature and evolution of the band-edge states in MoS<sub>2</sub>: From monolayer to bulk". In: *Phys. Rev. B* 90 (20 Nov. 2014), p. 205420. DOI: 10.1103/PhysRevB.90.205420 (cit. on p. 37).
- [119] Stock photo and royalty-free images on Fotolia.com - Pic 128894654. *sp3 sp<sub>2</sub> sp hybrid orbitals*. 2016. URL: <https://www.fotolia.com/id/128894654> (visited on 05/25/2017) (cit. on p. 38).
- [120] C.A. Coulson and W.E. Moffitt. "I. The properties of certain strained hydrocarbons". In: *Phil. Mag.* 40.300 (1949), pp. 1–35. DOI: 10.1080/14786444908561208 (cit. on p. 38).
- [121] Tobias Wassmann et al. "Clar's Theory,  $\pi$ -Electron Distribution, and Geometry of Graphene Nanoribbons". In: *J. Am. Chem. Soc.* 132.10 (Mar. 2010), pp. 3440–3451. DOI: 10.1021/ja909234y (cit. on p. 40).
- [122] Thomson/Brooks Cole. *Double bond*. 2004. URL: [http://images.slideplayer.com/14/4339766/slides/slide\\_7.jpg](http://images.slideplayer.com/14/4339766/slides/slide_7.jpg) (visited on 04/21/2017) (cit. on p. 40).
- [123] Zhirong Liu, Jinying Wang, and Jianlong Li. "Dirac cones in two-dimensional systems: from hexagonal to square lattices". In: *Phys. Chem. Chem. Phys.* 15 (43 2013), pp. 18855–18862. DOI: 10.1039/C3CP53257G (cit. on p. 42).
- [124] Jinying Wang et al. "The rare two-dimensional materials with Dirac cones". In: *Natl. Sci. Rev.* 2.1 (Mar. 2015), pp. 22–39. DOI: 10.1093/nsr/nwu080 (cit. on p. 42).
- [125] Yasumasa Hasegawa et al. "Zero modes of tight-binding electrons on the honeycomb lattice". In: *Phys. Rev. B* 74 (3 July 2006), p. 033413. DOI: 10.1103/PhysRevB.74.033413 (cit. on p. 42).
- [126] G J Ackland, M C Warren, and S J Clark. "Practical methods in ab initio lattice dynamics". In: *J. Phys. Condens. Matter* 9.37 (Sept. 1997), pp. 7861–7872. DOI: 10.1088/0953-8984/9/37/017 (cit. on p. 44).
- [127] K. Parlinski. "Phonons calculated from first-principles". In: *École thématique la Société Française la Neutron*. 12 (June 2011), pp. 161–166. DOI: 10.1051/sfn/20112008 (cit. on p. 44).

- [128] Atsushi Togo and Isao Tanaka. "First principles phonon calculations in materials science". In: *Scripta Materialia* 108 (2015), pp. 1–5. DOI: <https://doi.org/10.1016/j.scriptamat.2015.07.021> (cit. on p. 47).
- [129] J.F. Nye. *Physical Properties of Crystals: Their Representation by Tensors and Matrices*. Oxford science publications. For example: Clarendon Press, 1985 (cit. on p. 48).
- [130] Konstantin N. Kudin, Gustavo E. Scuseria, and Boris I. Yakobson. " $C_2F$ ". In: *Phys. Rev. B* 64 (23 Nov. 2001), p. 235406. DOI: [10.1103/PhysRevB.64.235406](https://doi.org/10.1103/PhysRevB.64.235406) (cit. on p. 49).
- [131] M. Topsakal, S. Cahangirov, and S. Ciraci. "The response of mechanical and electronic properties of graphane to the elastic strain". In: *Applied Physics Letters* 96.9 (2010), p. 091912. DOI: [10.1063/1.3353968](https://doi.org/10.1063/1.3353968) (cit. on p. 49).
- [132] Simone Bertolazzi, Jacopo Brivio, and Andras Kis. "Stretching and Breaking of Ultrathin MoS<sub>2</sub>". In: *ACS Nano* 5.12 (2011). PMID: 22087740, pp. 9703–9709. DOI: [10.1021/nn203879f](https://doi.org/10.1021/nn203879f) (cit. on p. 49).
- [133] Ryan C. Cooper et al. "Nonlinear elastic behavior of two-dimensional molybdenum disulfide". In: *Phys. Rev. B* 87 (3 Jan. 2013), p. 035423. DOI: [10.1103/PhysRevB.87.035423](https://doi.org/10.1103/PhysRevB.87.035423) (cit. on p. 49).
- [134] Cambridge University Engineering Department. *Materials Data Book*. 2003. URL: <http://www-mdp.eng.cam.ac.uk/web/library/enginfo/cueddatabooks/materials.pdf> (visited on 05/31/2017) (cit. on p. 49).
- [135] Max Born. "On the stability of crystal lattices. I". In: *Mathematical Proceedings of the Cambridge Philosophical Society* 36.2 (1940), pp. 160–172. DOI: [10.1017/S0305004100017138](https://doi.org/10.1017/S0305004100017138) (cit. on p. 49).
- [136] Félix Mouhat and François-Xavier Coudert. "Necessary and sufficient elastic stability conditions in various crystal systems". In: *Phys. Rev. B* 90.22 (Dec. 2014), p. 224104. DOI: [10.1103/PhysRevB.90.224104](https://doi.org/10.1103/PhysRevB.90.224104) (cit. on p. 49).